Nutritional control of cell size by the greatwall-endosulfine-PP2A·B55 pathway

Nathalia Chica[1,3], Ana Elisa Rozalén[1,3], Livia Pérez-Hidalgo[1,3], Angela Rubio[1], Bela Novak[2] and Sergio Moreno[1,4]

[1] Instituto de Biología Funcional y Genómica
CSIC / University of Salamanca
37007 Salamanca, Spain

[2] Oxford Centre for Integrative Systems Biology
Department of Biochemistry
University of Oxford
Oxford OX1 3QU, UK

[3] These authors contributed equally to the work

[4] Correspondence: smo@usal.es

Word count (excluding summary, references and figure legends): 4,827

Running title: Nutritional control of cell size

Keywords: Cell size; Cell cycle; TOR; Greatwall; Endosulfine; PP2A; B55; Igo1; Ppk18; *S. pombe*

Abstract

Proliferating cells adjust their cell size depending on the nutritional environment. Cells are large in rich media and small in poor media. This physiological response has been demonstrated in both unicellular and multicellular organisms. Here we show that the greatwall-endosulfine (Ppk18-Igo1, in fission yeast) pathway couples the nutritional environment to the cell cycle machinery by regulating the activity of PP2A·B55. In the presence of nutrients, greatwall (Ppk18) protein kinase is inhibited by TORC1 and PP2A·B55 is active. High levels of PP2A·B55 prevent the activation of mitotic Cdk1·Cyclin B and cells increase in size in G2 before they undergo mitosis. When nutrients are limiting, TORC1 activity falls off and the activation of greatwall (Ppk18) leads to the phosphorylation of endosulfine (Igo1) and inhibition of PP2A·B55, which in turn allows full activation of Cdk1·CyclinB and entry into mitosis with a smaller cell size. Given the conservation of this pathway, it is reasonable to assume that this mechanism operates in higher eukaryotes as well.

Introduction

Rod-shaped fission yeast cells are convenient for studying cell size control because they grow by tip elongation, maintaining a constant diameter [1]. Therefore, cell volume is proportional to cell length. In a classic paper published 39 years ago, Fantes and Nurse [2] described that in fission yeast the cell size necessary for cell division is determined by the growth conditions. When fission yeast cells are shifted from a nitrogen-rich to a nitrogen-poor medium, they are advanced into mitosis and divide at a smaller cell size. By contrast, when they are shifted from a nitrogen-poor to a nitrogen-rich medium cell size increases. Thus, fission yeast cells are large in nitrogen-rich media and small in nitrogen-poor media. This finding has been shown to be true also in proliferating tissue culture cells [3,4] and in multicellular organisms; for instance, wild-type flies fed under nutrient-limiting conditions develop to approximately half the size of their well-fed counterparts [5]. This reduction in body size is caused by a decrease in cell size rather than in cell numbers. The molecular mechanism underlying this response is poorly understood.

The regulation of cell growth by nutrients is controlled by the highly conserved TORC1 pathway, which promotes growth by enhancing anabolic processes, including ribosome biogenesis and protein translation, while inhibiting catabolic processes, such as autophagy and the general stress response [6]. Here we show that in wild-type fission yeast cells growing in rich medium TORC1 is a powerful inhibitor of the greatwall-endosulfine (Ppk18-Igo1) pathway, hence allowing full activity of PP2A·B55 which, as in *Drosophila*, *Xenopus* and mammalian cells, counteracts CDK activity in G2 [7-9], resulting in larger cells. However, when these cells are shifted to poor medium, the down-regulation of TORC1 allows the activation of greatwall (Ppk18), which phosphorylates endosulfine (Igo1) to inhibit PP2A·B55, resulting in premature CDK activation and accelerated entry into mitosis. Accordingly, we provide a simple mechanism for coupling cell size to the nutritional environment by modulating the activity of the greatwall-endosulfine-PP2A pathway on the cell cycle machinery.

Results

The fission yeast endosulfine Igo1 is required to advance entry into mitosis upon nutritional shift-down

Fission yeast monitors its cell size at the end of G1 (G1/S size control) and at the end of G2 (G2/M size control or mitotic size control) [2,10,11]. In wild-type cells growing in nitrogen-rich medium (yeast extract or minimal medium with ammonium chloride or glutamate as a nitrogen source), the size threshold to enter mitosis is high, and the G1/S size control is cryptic because cell division produces daughter cells with a size greater than the minimum required to initiate S-phase. In these conditions, G2 is long and G1 is short [10-12]. However, the cell size threshold to enter mitosis is greatly reduced when wild-type cells are shifted to medium with a poor nitrogen source, such as minimal medium with proline [2,13], isoleucine or phenylalanine [14]. In these conditions, wild-type cells initiate mitosis at a reduced cell size, generating two daughter cells that are smaller than the critical size threshold required to progress through G1/S [2,12] (Figures 1A and 1B). These small cells grow during G1 in order to reach the G1/S size threshold and they show a 1C G1 population (Figure 1C, wild-type). We identified *igo1/mug134*, encoding the fission yeast endosulfine orthologue (*www.pombase.org*), as a gene involved in the nutritional response that advances

mitosis when cells are shifted from rich minimal medium with glutamate (MMGlu) to poor minimal medium with phenylalanine (MMPhe). Contrary to wild-type cells, *igo1Δ* mutant cells did not accelerate entry into mitosis after the nutritional shift-down. Instead, these mutant cells continued to grow in G2 and divided with a larger cell size than the wild-type (Figures 1A and 1B) and they did not show a 1C G1 population in minimal medium with either isoleucine (MMIle) or phenylalanine (MMPhe) (Figure 1C, *igo1Δ*). This suggests that in fission yeast Igo1 is part of the mechanism that advances cells into mitosis when nitrogen is limiting.

The fission yeast greatwall-endosulfine pathway is involved in the G2/M size control

Endosulfines are small phosphoproteins, highly conserved from yeasts to humans, which specifically bind to and inhibit the PP2A·B55 protein phosphatase subcomplex [8,9]. PP2A·B55 has been shown to be cell cycle-regulated in *Xenopus*, following the opposite pattern of activity to Cdk1·Cyclin B (high in interphase and low in mitosis) [15]. In higher eukaryotic cells, the phosphorylation of endosulfines (ENSA and Arpp19) by greatwall kinase (MASTL in mammalian cells) inhibits PP2A·B55 and promotes entry into mitosis [8,9]. Ppk18, Cek1 and Ppk31 are the fission yeast protein kinases with the highest degree of homology to greatwall. Cells deleted for *ppk31* behaved essentially like the wild-type when they were grown in MMPhe (data not shown), whereas cells deleted for *cek1* also reduced their cell size, albeit to a lesser extent than the wild-type (Figure 1D). On the contrary, cells deleted for *ppk18Δ* and the double mutant *ppk18Δ cek1Δ* did not undergo a reduction in cell size, and their cell length and DNA content in MMPhe was similar to that of the *igo1Δ* mutant (Figures 1D-1F). These results are consistent with the idea that Ppk18 and Igo1 are required to promote entry into mitosis upon nitrogen deprivation and that Ppk18 is the main fission yeast greatwall kinase, whereas Cek1 could play a minor role as a greatwall kinase.

The Ppk18-Igo1 signalling pathway acts upstream from PP2A and promotes entry into mitosis

In fission yeast two genes, *ppa1* and *ppa2,* encode the catalytic subunit of PP2A and one gene, *pab1*, the B55 regulatory subunit [16,17]. Deletion of *ppa2* is viable and shows a semi-*wee* phenotype, whereas deletion of *ppa1* is only slightly smaller than

the wild-type [16] (Figure 2A), suggesting that Ppa2 plays a major role and Ppa1 a minor role in regulating the G2/M transition. The double mutant *ppa1Δ ppa2Δ* is lethal, producing small *wee* cells that die by mitotic catastrophe [16]. Consistent with a role of PP2A·B55 as a negative regulator of the G2/M transition, reduced expression of *pab1* (B55) from the thiamine repressible *nmt1* promoter (version 41) also generated cells smaller than the wild-type (Figures 2B and 2C).

Ppa2 interacts genetically with the cycle regulators *wee1* and *cdc25*, because the *ppa2Δ* mutant is lethal in combination with *wee1-50* and partially suppresses the *cdc25-22* temperature-sensitive (ts) alleles [18,19] (our unpublished results). Consistent with these data, deletion of *igo1Δ* generated the opposite phenotypes; *igo1Δ* suppressed the phenotype of *wee1-50* and enhanced the elongated and ts phenotype of *cdc25-22* (Figure S1). Double mutants *igo1Δ ppa2Δ* or *igo1Δ nmt1(41):pab1* displayed a small cell size in MMGlu containing thiamine, similar to the size of the *ppa2Δ* single mutant (Figure 2D), suggesting that Igo1 operates upstream from Ppa2 and Pab1.

Moderate overexpression of Ppk18 promotes entry into mitosis

If Ppk18 (greatwall) and Igo1 (endosulfine) act on the same pathway to inhibit PP2A, then the hyperactivation of Ppk18 should advance entry into mitosis, generating small cells, even in rich medium. In order to test this hypothesis, we overexpressed *ppk18* in cells growing in rich medium (MMGlu). Moderate overexpression of *ppk18* generated small cells (Figure 3A), with a phenotype reminiscent of the *cdc25* overexpression [20] or the inactivation of *wee1* [21]. This phenotype was dependent on the presence of Igo1, since overexpression of *ppk18* in cells lacking Igo1 did not undergo a reduction in cell size (Figure 3A). Moreover, cells overexpressing *ppk18* showed a cell cycle delay in G1 (Figure 3B), indicating that moderate overexpression of *ppk18* only affects the G2/M and not the G1/S size control. Moderate overexpression of *cek1* from the same promoter has only a minor effect on cell size reduction (11.37±0.92) compared with overexpression of *ppk18* (8.88±0.90) and did not generate cells with 1C DNA content (Figures 3A and 3B). Taken together, these results suggest that Ppk18 and Igo1 are positive regulators of the G2/M transition in fission yeast.

Igo1 is rapidly phosphorylated at serine 64 upon nitrogen deprivation or starvation

In *Xenopus* and mammalian cells, phosphorylation of ENSA by greatwall at serine 67 promotes its binding to and inhibition of PP2A·B55 phosphatase [8,9]. The equivalent serine in Igo1 is serine 64 (Figure 4A). We raised antibodies to the C-terminal peptide (C-GASSRRESVTRHDLE) and to a peptide containing the phospho-Ser64 epitope (C-GRKYFD**Sp**GDYALNNK) in Igo1. Using these antibodies, we found that the levels of Igo1 protein and of phosphorylated Igo1 at Ser64 increased when wild-type cells were shifted from MMGlu to MMPhe (Figure 4B and Table S1). The phosphorylated band was not detected in the *igo1-S64A* mutant (Figure 4B) and this mutant showed a phenotype similar to the *igo1Δ* (Figures 4C and 4D). These results indicate that the greatwall-endosulfine pathway is activated in response to nitrogen deprivation in fission yeast.

Phosphorylation of Igo1 was severely impaired in cells deleted for *ppk18* or expressing a kinase dead version of *ppk18* (*ppk18-K595A* or *ppk18-KD*) but was still present in *cek1* deleted cells (Figure 4B), consistent with the idea that Ppk18 is the main greatwall kinase that phosphorylates Igo1 in medium with low nitrogen.

In order to investigate the kinetics of Igo1 phosphorylation we performed a time-course experiment on cells shifted from MMGlu to MMPhe. As indicators of the nutritional shift-down, we determined the decrease in the phosphorylation of fission yeast ribosomal protein S6 (Rps6) [22] and the increase in the Ser52 phosphorylation of eukaryotic initiation factor 2α (eiF2α[23]. As shown in Figure 4E, the levels of Igo1 phosphorylated at Ser64 increased rapidly by 1 hour after the shift, with a kinetic similar to the phosphorylation of eiF2α at Ser52. The phosphorylation of Igo1 at Ser64 was fully dependent on Ppk18, since cells lacking this kinase were unable to phosphorylate Igo1 (Figure 4F). We also counted the percentage of cells in mitosis (cells in anaphase after DAPI staining) and the percentage of cells dividing (cells septating after blankophor staining) in wild-type, *igo1Δ* and *igo1-S64A* mutant cells. In agreement with previously published data [2,13] we observed a peak of mitotic cells 80 minutes after the shift in the wild-type, which was followed by another peak of dividing cells at 120 minutes (Figures 4G and 4H and Movie S1), which correspond to the population the cells that were advanced into mitosis. These peaks were absent in the *igo1Δ* and in the *igo1-S64A* mutant (Figures 4G and 4H and Movie S2). Moreover, a

peak in G1 cells (1C DNA content) was observed 4 hours after the shift only in the wild-type, and not in *igo1Δ, igo1-S64A* or *ppk18Δ* mutants (Figure 4I). Together, these data indicate that upon nitrogen shift-down the Ppk18-dependent Igo1 phosphorylation at Ser64 is required to accelerate mitotic entry and cell division, resulting in small cells with a G1/S and G2/M size control.

We next performed a complete nitrogen starvation experiment by shifting wild-type and *igo1Δ* mutant cells from MMGlu to MM without nitrogen (MM-N). Ppk18-dependent phosphorylation of Igo1 was observed 30 minutes after the shift in wild-type cells (Figure 4J). These cells underwent cell division and a reduction in cell size, and they eventually arrested in G1. By contrast, this nutritional response was abolished in *igo1Δ, igo1-S64A* and *ppk18Δ cek1Δ* cells (Figure S2). As a consequence, *igo1Δ* mutant cells remained in G2 and mating efficiency was reduced to approximately 50% of the wild-type (Figure 4K). A short G2 and a long G1 are advantageous for fission yeast cells when nutrients are scarce because only G1 cells can mate and form spores that can survive starvation. Therefore, the Ppk18-Igo1 pathway allows an optimal response to nitrogen starvation, an acceleration of mitosis, and G1 arrest prior to conjugation.

The Ppk18-Igo1-PP2A pathway links TOR to mitotic size control

In budding yeast, the greatwall orthologue Rim15 is required for entry and survival in G0 stationary phase [24,25], for extension of the chronological life-span [26] and for gametogenesis [27]. Upon nutrient limitation, Rim15 enters the nucleus and phosphorylates the endosulfine paralogues Igo1 and Igo2 [28], which directly inhibit PP2A·Cdc55, maintaining the Gis1 transcription factor in an active phosphorylated state, which promotes the expression of target genes required for the survival in G0 [28]. Rim15 integrates signals from nutrient-dependent protein kinases (PKA, TORC1 and Pho85), which inhibit its activity. In response to nitrogen, TORC1 promotes the phosphorylation and inhibition of Rim15 [25].

We tested whether, as in budding yeast, the fission yeast Ppk18 is negatively regulated by TORC1. First, we used a temperature-sensitive allele of *tor2* (the catalytic subunit of TOR complex 1, TORC1). The *tor2-51* mutant grows and divides like the wild-type at 25ºC. However, when shifted to 35ºC *tor2-51* mutant cells stop growth, undergo

premature entry into mitosis, cell size reduction and cell cycle delay in G1, reminiscent of the nitrogen starvation response [29]. When wild-type and *tor2-51* mutant cells were shifted from 25 to 35ºC, Ppk18-dependent phosphorylation of Igo1 in the *tor2-51* mutant was detected only at 35ºC but not at 25ºC (Figure 5A), suggesting that TORC1 negatively regulates Ppk18 in fission yeast. As expected, the temperature-sensitive *tor2-51* mutant showed a reduced cell size at 35ºC (Figure 5B). However, the size of *tor2-51 igo1Δ* double mutant was greater than *tor2-51* and closer to the size of the wild-type or the *igo1Δ* (Figure 5B), indicating that Igo1 is required for the reduction in cell size after TORC1 down-regulation.

Rapamycin and Torin, two well-characterised TOR inhibitors, also induced activation of the Ppk18-Igo1 pathway (Figures 5C and 5D). Phosphorylation of Igo1 at Ser64 was detected as early as 30 minutes after the addition of the drugs, in parallel with the reduction in S6 kinase activity, and was dependent on the presence of Ppk18 (Figures 5C and 5D). In sum, these results indicate that, as in budding yeast, fission yeast TORC1, which responds mainly to nitrogen, inhibits the greatwall-endosulfine pathway.

Therefore, active TORC1, in nitrogen-rich medium, allows the full activation of PP2A·B55 by inactivating Ppk18-Igo1. High PP2A·B55 activity sets the G2/M size threshold at maximum levels by inhibiting the Cdc25 mitotic activator and activating the Wee1 mitotic inhibitor. When nutrients are reduced, inactivation of TORC1 allows the activation of Ppk18-Igo1 to decrease the activity of PP2A·B55, promoting the acceleration of the G2/M transition.

Sck2 S6 kinase negatively regulates Ppk18

TORC1 phosphorylates and activates the budding yeast S6 kinase orthologue Sch9, which in turn phosphorylates and inhibits Rim15 [25,30]. In fission yeast, there are three protein kinases highly related to budding yeast Sch9 and S6 kinase in animal cells: Sck1, Sck2 and Psk1 [22]. In order to test if any of these kinases play a role on cell size regulation in fission yeast we measured the cell size of mutants lacking or overexpressing *sck1*, *sck2* and *psk1*. Cells lacking *sck2* were shorter and cells overexpressing *sck2* were larger than the wild-type cells in rich medium [31] (Figure 6A). Overexpression of *sck2*, and to a lesser extent overexpression of *sck1*, inhibited Ppk18 activity *in vivo* in cells growing in MMPhe where Ppk18 is active (Figure 6B,

lanes 4 and 6), suggesting that Sck2 (and to a lesser extent Sck1) could phosphorylate and inactivate Ppk18. Consistent with this result, fission yeast cells lacking Sck2 showed increased phosphorylation of Igo1 compared to the wild-type in nitrogen-rich medium (Figure S3).

Phosphoproteomic analyses have shown that Ppk18 is highly phosphorylated *in vivo* in cells growing in rich medium [32,33]. The Ppk18 protein sequence contains several potential phosphorylation sites for S6 kinase (RXRXX[ST]; S1010, S1012, and S1020) and for protein kinase A ([RK][RK]X[ST]; S498, T587, S1020, and S1141). Mutation of these sites to alanine (ppk18-2A^{S6K} -S1010A S1012A-, ppk18-4A$^{PKA/S6K}$ -S498A T587A S1020A S1141A- and ppk18-6A$^{PKA/S6K}$ -S498A T587A S1010A S1012A S1020A S1141A-) resulted in a progressive decrease in cell size (Figure 6C), and a progressive increase in Igo1-S64 phosphorylation (Figure 6D and Table S1), suggesting a negative role of the S6 kinase and PKA on Ppk18 activity (Figure 6C and 6D). Together, these results indicate that fission yeast Sck2 kinase could phosphorylate and inhibit Ppk18 in nitrogen-rich medium.

Ppk18 phosphorylates Igo1 at serine 64 to inhibit PP2A·B55

Our genetic and physiological data is in agreement with published work in budding yeast, *Drosophila*, *Xenopus* and mammalian cells indicating that greatwall phosphorylates endosulfine to inhibit PP2A·B55 [8,9,27,28,35]. To test whether Igo1 is a direct target of Ppk18, we performed Ppk18 *in vitro* kinase assays using purified recombinant Igo1 and Igo1-S64A, as substrates. Extracts from wild-type (*ppk18^{+})* and Myc-tagged Ppk18 (*ppk18-13myc*) cells, treated for 1 hour with rapamycin in order to activate Ppk18, were immunoprecipitated with anti-c-Myc monoclonal antibodies. Ppk18-13myc immunoprecipitates were able to phosphorylate *in vitro* wild-type Igo1 but not Igo1-S64A (Figure S4A), indicating that fission yeast Ppk18 can act as a greatwall kinase.

To determine whether Ser64-phosphorylated Igo1 inhibits the PP2A·B55 (PP2A·Pab1 in fission yeast) phosphatase activity, PP2A·Pab1 phosphatase was purified from cells expressing GST-Pab1 using glutathione sepharose beads and assayed for phosphatase activity. Wild-type Igo1 thiophosphorylated *in vitro* at Ser64 by *Xenopus* Greatwall, but not Igo1-S64A, inhibited more than 90% the phosphatase activity of PP2A·Pab1 (B55)

(Figure S4B and S4C). This result indicates that Ser64-phosphorylated Igo1 inhibits the activity of PP2A·B55, analogous to the situation in budding yeast [27,28,35] and animal cells [8,9].

The greatwall-endosulfine pathway works independently of Sty1 and Pom1-Cdr1/2

Two pathways, the Sty1 (also known as Spc1 or Phh1) stress response MAP kinase pathway and the cell geometry-sensing Pom1 kinase pathway, regulate the activity of Wee1 and Cdc25 in fission yeast. Sty1 can be activated by nutrient deprivation to advance entry into mitosis by phosphorylating and recruiting the Polo kinase (Plo1) to the spindle-pole body, where it activates Cdk1 [13,36]. The activity of Sty1 is in balance between the activating phosphorylation by Wis1 MAP kinase kinase and the inhibitory dephosphorylation by Pyp1 and Pyp2 phosphatases [37,38]. Nitrogen shift-down from glutamate to proline (but not complete nitrogen starvation) reduces the activity of the Pyp2 phosphatase, which seems to be responsible for Sty1 activation [13]. The cell geometry pathway maintains Wee1 active until the cell reaches a certain length. Cdr1 and Cdr2 are two Wee1-inhibitory kinases located in the cortical nodes in the middle of the cell, which are themselves inhibited by Pom1, another kinase that is present as a gradient along the long axis of the cell. In G2, Pom1 inhibits Cdr1 and Cdr2 and Wee1 is active. When the cell reaches a certain size, Pom1 located at the poles no longer inhibits Cdr1 and Cdr2 and Wee1 is inhibited, triggering mitosis [39,40].

In order to test whether PP2A, Sty1 and Pom1 are on the same pathway or not, Navarro and Nurse [18] measured the length of the double mutants *ppa2Δ sty1Δ* and *ppa2Δ cdr1Δ* and compared them with the length of the single mutants. Deletion of *ppa2*Δ reduced the cell size of both the *sty1Δ* and *cdr1Δ* cells, indicating that Ppa2 acted in G2 independently of Sty1 and Cdr1. Moreover, the double *cdr1Δ sty1Δ* mutant was viable and divided with a larger size than any of the parental strains [18]. We have reached similar conclusions, since the double mutants *igo1Δ sty1Δ* and *igo1Δ cdr1Δ* (Table S2) were larger than the single mutants, indicating that the greatwall-endosulfine pathway functions independently of the Sty1 and the Pom1-Cdr1/Cdr2 pathways to regulate cell size at division.

Mathematical modelling

Our data suggest that the greatwall-endosufine-PP2A pathway regulates mitotic commitment in fission yeast by counteracting Cdk1 auto-activation controlled by inhibitory phosphorylation. This proposal was tested by extending a mathematical model of the fission yeast cell cycle [41] with a kinetic description of the greatwall-endosufine-PP2A (Figures 7A and S5A). The numerical simulations of wild-type and *igo1Δ* cell cycles are shown in Figure S5B-S5E. Wild-type cells become smaller in poor medium, while *igo1Δ* mutants divide at a larger size. Therefore the G1 phase corresponding to high levels of Cdk1 inhibitor (Rum1) is extended in poor medium for the wild-type but not for *igo1Δ* mutants.

Since cell cycle progression is driven by cytoplasmic growth and is regulated by size-control mechanisms, it is convenient to plot Cdk1 activity as a function of cell size instead of time. Three stable steady states (solid lines) with low, intermediate and high Cdk1·Cdc13 activities become apparent in different cell size ranges (Figure 7B). The low Cdk1 activity state (red segment), observable at small cell size, is stabilized by Rum1 and corresponds to 'G1 arrest'. Inhibitory Cdk1 phosphorylation is responsible for the steady state with intermediate Cdk1 activity of the S/G2 phase (yellow segment). The high Cdk1 activity state (green segment) becomes destabilized (dashed line) in large cells by Cdk1-activated APC/C-dependent Cdc13 degradation. The right edge of the low and intermediate Cdk1 steady states represents the size thresholds for the S and M phases, respectively. Activation of Cdk1 auto-regulatory loops delays the G2/M transition above the threshold size of mitosis.

In rich medium, during the interphase of wild-type cells PP2A activity is close to its maximum value observable in *igo1Δ* mutants (Figures S5B and S5C). High PP2A activity raises the mitotic size threshold by opposing the phosphorylation of Wee1 and Cdc25 by Cdk1. Therefore, wild-type cells in rich medium and *igo1Δ* mutants in both rich and poor media divide at a large size, and give birth to cells above the critical size for S phase, which makes G1/S size-control cryptic (blue trajectories on Figures 7B and 7C). When cells are shifted to poor medium, greatwall inhibition TOR is partially lifted, which results in an inhibition of PP2A by Igo1 in wild-type cells. PP2A inhibition reduces the mitotic size threshold, which allows G2 phase cells to activate Cdk1 prematurely and enter into M phase (Figure 7D).

Discussion

Here we show that the greatwall (Ppk18)-endosulfine (Igo1)-PP2A pathway is part of the mechanism that links cell growth with cell division to maintain cell size homeostasis in fission yeast. In multicellular organisms, the greatwall-endosulfine pathway promotes entry into mitosis by inhibiting the PP2A·B55 protein phosphatase [8,9], which dephosphorylates Cdk1·Cyclin B target proteins, including Cdc25 and Wee1 [42,43], thus preventing the autocatalytic amplification of Cdk1·Cyclin B [44]. In budding yeast, Rim15 (greatwall) and its substrates Igo1 and Igo2 (endosulfines) are required for G1 arrest [45] and entry into quiescence (G0) in response to nutritional deprivation by promoting the expression and stability of specific genes that are important for the G0 program [27,28,46]. This pathway in budding yeast is also required for timely entry into mitosis under temperature stress [35]. However, in *S. cerevisiae*, PP2A·B55 promotes, rather than prevents, entry into mitosis [47], which is the opposite to the role of PP2A·B55 in animal cells and fission yeast.

We have also found that fission yeast greatwall (Ppk18) is under nutritional control by TORC1. When nitrogen is abundant, active TORC1 inactivates greatwall (Ppk18) by phosphorylation, presumably by activating the Sck2 S6 kinase, and PP2A·B55 is active. Thus, cells grow to a larger size in G2 before they enter mitosis. When nutrients are scarce, TORC1 and Sck2 activity drop off, relieving the inhibition on greatwall (Ppk18), which now phosphorylates endosulfine (Igo1) to inhibit PP2A·B55. Low PP2A·B55 activity allows entry into mitosis with a reduced size. Thus, fission yeast greatwall (Ppk18) and endosulfine (Igo1) are required for the advancement of mitotic onset and cell size reduction that take place after nutrient deprivation or starvation (Figure 7).

In agreement with this idea, moderate overexpression of greatwall (Ppk18) in rich medium (MMGlu) generated small cells (Figures 3A and 3B), similar to the overexpression of *cdc25* [20] or the lack of *wee1* [21], indicating that the activity of greatwall is rate-limiting for entry into mitosis. These cells expressing high levels of Ppk18 underwent cell division with a shorter G2 and a longer G1 than the wild-type, presumably because the increase in Ppk18 levels titrates out its endogenous upstream negative regulators, TORC1 and Sck2. Collectively, these observations suggest that

entry into mitosis is promoted by the combined activation of Cdk1·Cyclin B and inactivation of PP2A·B55. Thus, in poor medium the greatwall-endosulfine pathway tilts the Cdk1·Cyclin B / PP2A·B55 balance to accelerate entry into mitosis.

The TOR pathway also controls cell size in *Drosophila* and mammalian cells. Flies fed with a nutrient-restricted diet are small, as a consequence of a reduction in cell size rather than in cell number [5]. Loss of function mutations in *Drosophila* and mice S6 kinase 1 (S6K1) lead to smaller animals with smaller cells [5,48]. Inhibition of TOR with rapamycin or by silencing mTOR or Raptor in tissue culture cells reduces cell size in many cell types, including HEK293T [4], rat1.a fibroblasts and U2OS human osteosarcoma cells [3]. Together, these experiments clearly indicate that the function of TOR-S6 kinase in cell size control is evolutionarily conserved in flies and mammals. Therefore, it will be important in the future to test whether the mechanism described here is also conserved in multicellular organisms.

Experimental Procedures

Fission yeast strains and methods

The fission yeast strains used in this study are listed in Supplemetary Experimental Procedures. Fission yeast cells were grown and manipulated genetically according to standard protocols [49]. Genetic crosses were performed on malt extract agar plates (MEA). Cells were typically grown overnight at the appropriate temperatures in yeast extract supplemented with adenine, leucine, histidine, lysine and uracil (YES) and then transferred to Edinburgh minimal medium containing either 93.5 mM ammonium chloride (EMM) or 20 mM glutamate (MMGlu), as a nitrogen source. For nutritional shift-down experiments, cells growing in MMGlu were transferred to minimal medium containing 20 mM phenylalanine (MMPhe), 20 mM Isoleucine (MMIle) or to minimal medium without nitrogen (MM-N). In all cases, cells grown to mid-exponential phase ($5x10^6$ – $8x10^6$ cells/ml) were centrifuged and washed three times in the destination medium. Nitrogen starvation experiments were performed by shifting exponentially growing wild-type fission yeast cells from EMM to EMM without ammonium chloride. For Tor2 inactivation experiments, cells were grown in YES medium at 25ºC and shifted to 35ºC for 4 hours. Rapamycin (Sigma-Aldrich) was added to fission yeast cells growing in YES to a final concentration of 220 nM from a stock solution of 110 µM in DMSO. Cells treated only with DMSO were used as controls. Torin was added at a concentration of 25 µM from a stock solution of 7.5 mM in DMSO. All experiments were performed with prototrophic strains to avoid the addition of supplements (amino acids or uracil) to the minimal medium, which could be used as a nitrogen source.

nmt1 constructions

A PCR-based strategy was used to insert the nmt1(41) promoter to express GFP fused to Ppk18 at the *ppk18*$^+$ genomic locus [50], the nmt1(41) promoter at the *cek1*$^+$ genomic locus, and the nmt1 promoter at the *sck1*$^+$, *sck2*$^+$, and *psk1*$^+$ genomic loci. Oligonucleotides with 80 bases of homology to regions flanking the respective initiation codons were used to amplify the P41nmt1-GFP-kanMX6, P41nmt1-kanMX6, and P3nmt1-kanMX6 sequences from plasmids pFA6a-P41nmt1-GFP-kanMX6, pFA6a-P41nmt1-kanMX6, and pFA6A-P3nmt1-kanMX6, and the PCR products were used to transform a wild-type strain *h- 972*. Cells expressing *nmt1(41):GFP:ppk18, nmt1(41):cek1, nmt1:sck1, nmt1:sck2* or *nmt1:psk1* constructions were grown on YES

and then transferred to MMGlu containing 5 µg/ml of thiamine to repress expression from the *nmt1* promoter. For induction, cells were washed 3 times in MMGlu and incubated overnight at 25ºC in MMGlu.

Site-directed mutagenesis of *igo1*$^{+}$

The 1,1 Kb *BamH*I-*EcoR*I genomic fragment containing the *igo1+* gene flanked by endogenous promoter and terminator sequences was cloned from genomic DNA into *pBluescriptSK+* to obtain pBS-*igo1*$^{+}$. Site-directed mutagenesis by PCR was performed to change the serine 64 to alanine using the *QuikChange* II *XL Site- Directed Mutagenesis Kit* (Agilent Technologies). The resulting plasmid was pBS-*igo1-S64A*, which was confirmed by DNA sequencing. The *BamH*I-*EcoR*I fragment was isolated by digestion and used to transform the *h- igo1::ura4*$^{+}$ (S2339) strain. After 5-fluoro-orotic acid counter-selection, *S. pombe* transformants of mutagenized *igo1*$^{+}$ were identified and further confirmed by PCR analysis followed by direct sequencing of PCR products.

Site-directed mutagenesis of *ppk18*$^{+}$

The *ppk18*$^{+}$ gene flanked by endogenous promoter and terminator sequences was amplified from genomic DNA and cloned into pGEM-T-easy to obtain pGEM-T-easy-*ppk18*$^{+}$. Plasmids pGEM-T-easy-ppk18^{K595A} (kinase dead 'KD'), pGEM-T-easy-ppk18$^{S1010A/S1012A}$ ('2A-S6K'), pGEM-T-easy-ppk18$^{S498A/T587A/S1020A/S1141A}$ ('4A-PKA/S6K'), and pGEM-T-easy-ppk18$^{S498A/T587A/S1010A/S1012A/S1020A/S1141A}$ ('6A-PKA/S6K'), were constructed by site-directed mutagenesis by PCR with the QuikChange II XL Site-Directed Mutagenesis Kit (Agilent Technologies). Mutations were confirmed by DNA sequencing and, after plasmid digestion, DNA fragments containing the mutated gene were used to transform the *h*$^{+}$ *ppk18::ura4*$^{+}$ *ura4-D18 leu1-32 ade6-M210* (S2460) strain. Fission yeast transformants containing the mutagenized *ppk18*$^{+}$ were identified by 5-fluoro-orotic acid counter-selection and further confirmed by PCR analysis and sequencing.

Cell size measurements

200 µl of cells in the exponential phase were washed in PBS and resuspended in 3 µl of 50 µg/ml blankophor (Bayer) and 2µl of PBS and examined under a Nikon Eclipse 90i fluorescence microscope equipped with a Plan/Apo 60X oil objective lens and a Hamamatsu ORCA-ER Camera. Live images were acquired with MetaMorph software (Molecular Devices). Cell length was measured from pictures of 100 septated cells

using ImageJ (National Institutes of Health). Average cell length and standard deviations were determined in 100 cells, and comparison between strains was accomplished using an independent and paired sample t-test.

Statistical analysis

Student´s t test were used to calculate significance differences between two groups.

SUPPLEMENTAL INFORMATION

Detailed experimental procedures can be found in the Supplemental Information, including two movies, five figures, two tables, Supplemental Experimental Procedures, the code to the mathematical model and Supplemental References.

AUTHOR CONTRIBUTIONS

Conceived and designed the experiments: NC, LP-H and SM. Performed the experiments: NC, AER, AR, LP-H and SM. Analysed the data: NC, AER, AR, LP-H and SM. Made the mathematical model: BN. Wrote the paper: SM wrote the experimental part of the manuscript and BN wrote the mathematical model.

ACKNOWLEDGEMENTS

We thank all members of the S.M. laboratory for helpful discussions, in particular M. Tormos-Pérez. We are extremely grateful to S. Mochida and K. Takeda for sharing their work before publication. To S. Mochida for hosting S.M. in his laboratory and for his invaluable help to perform the Igo1 thiophosphorylation reactions and the PP2A-Pab1 phosphatase assays shown in Figure S4. To F. Navarro, P. Nurse, C. Rallis, S. Ruibal, K. Shiozaki, M. Tormos-Pérez, N. Valbuena and M. Yamamoto for strains; K. Gull for the anti-tubulin antibody, J. Botet for his help in the early stages of this work, T. Hunt, S. Mochida, J.M. Pereda and M. Sacristán for suggestions on the purification of Igo1 in *E.coli* and greatwall kinase assays and N. Skinner for corrections to the manuscript. This research was funded by grants from the Spanish Ministry of Economy and Competitiveness MINECO (CSD2007-0015, BFU2011-28274 and BFU2014-55439) and Junta de Castilla y León (CSI151U13). B.N. receives support from the EC 7th Framework Program (MitoSys-241548) and BBSRC sLoLa (BB/MM00354X/1). N.C. and A.R. were recipients of FPI predoctoral training grants from the MINECO.

References

1. Mitchison, J.M. (1977). The biology of the cell cycle. Cambridge University Press, London, UK.
2. Fantes, P., and Nurse, P. (1977). Control of cell size at division in fission yeast by a growth -modulated size control over nuclear division. Exp. Cell Res. *107*, 377-386.
3. Fingar, D.C., Salama, S., Tsou, C., Harlow, E., and Blenis, J. (2002). Mammalian cell size is controlled by mTOR and its downstream targets S6K1 and 4EBP1/eIF4E. Genes Dev. *12*, 1472-1478.
4. Kim, D.H., Sarbassov, D.D., Ali, S.M., King, J.E., Latek, R.R., Erdjument-Bromage, H., Tempst, P., and Sabatini, D.M. (2002). mTOR interacts with raptor to form a nutrient-sensitive complex that signals to the cell growth machinery. Cell *110,* 163-175.
5. Montagne, J., Stewart, M.J., Stocker, H., Hafen E., Kozma, S.C., and Thomas, G. (1999). *Drosophila* S6 kinase: a regulator of cell size. Science *285*, 2126-2129.
6. Loewith, R., and Hall, M.N (2011). Target of rapamycin (TOR) in nutrient signaling and growth control. Genetics *189,* 1177-1201.
7. Yu, J., Fleming, S.L., Williams, B., Williams, E.V., Li, Z., Somma, P., Rieder, C.L., and Goldberg ML.(2004). Greatwall kinase: a nuclear protein required for proper chromosome condensation and mitotic progression in *Drosophila*. J. Cell Biol. *164,* 487-492.
8. Mochida, S., Maslen, S.L., Skehel, M., and Hunt, T. (2010). Greatwall phosphorylates an inhibitor of protein phosphatase 2A that is essential for mitosis. Science *330,* 1670-1673.
9. Gharbi-Ayachi, A. Labbé, J.C., Burgess, A., Vigneron, S., Strub, J.M., Brioudes, E., Van-Dorsselaer, A., Castro, A., and Lorca, T. (2010). The substrate of Greatwall kinase, Arpp19, controls mitosis by inhibiting protein phosphatase 2A. Science *330***,** 1673-1677.
10. Fantes, P.A. (1977). Control of cell size and cycle time in *Schizosaccharomyces pombe*. J. Cell Sci. *24,* 51-67.
11. Nurse, P., and Thuriaux, P. (1977). Controls over the timing of DNA replication during the cell cycle of fission yeast. Exp. Cell Res. *107,* 365-375.
12. Nasmyth, K.A. (1979). A control acting over the initiation of DNA replication in the yeast *Schizosaccharomyces pombe*. J. Cell Sci. *36,* 155-68.
13. Petersen, J., and Nurse, P. (2007). TOR signalling regulates mitotic commitment through the stress MAP kinase pathway and the Polo and Cdc2 kinases. Nat. Cell. Biol. *9,* 1263-1272.
14. Carlson, C.R., Grallert, B., Stokke, T., and Boye, E. (1999). Regulation of the start of DNA replication in *Schizosaccharomyces pombe*. J. Cell Sci. *112,* 939-946.

15. Mochida, S., and Hunt, T. (2007). Calcineurin is required to release Xenopus egg extracts from meiotic M phase. Nature *449,* 336-340.
16. Kinoshita, N., Ohkura, H., and Yanagida, M. (1990). Distinct, essential roles of type 1 and 2A protein phosphatases in the control of the fission yeast cell division cycle. Cell *63,* 405-415.
17. Kinoshita, K., Nemoto, T., Nabeshima, K., Kondoh, H., Niwa, H., and Yanagida, M. (1996). The regulatory subunits of fission yeast protein phosphatase 2A (PP2A) affect cell morphogenesis, cell wall synthesis and cytokinesis. Genes Cells *1,* 29-45.
18. Navarro, F.J., and Nurse, P. (2012). A systematic screen reveals new elements acting at the G2/M cell cycle control. Genome Biol. *13,* R36.
19. Kinoshita, N., Yamano, H., Niwa, H., Yoshida, T., and Yanagida, M (1993). Negative regulation of mitosis by the fission yeast protein phosphatase ppa2. Genes Dev. *7,* 1059-1071.
20. Russell, P., and Nurse, P. (1986). *cdc25* functions as an inducer in the mitotic control of fission yeast. Cell *45,* 145-153.
21. Nurse, P. (1975). Genetic control of cell size at cell division in fission yeast. Nature *256,* 547-551.
22. Nakashima, A., Sato, T., and Tamanoi, F. (2012). Fission yeast TORC1 regulates phosphorylation of ribosomal S6 proteins in response to nutrients and its activity is inhibited by rapamycin. J. Cell Sci. *123,* 777-786.
23. Valbuena, N, Rozalén, A.E., and Moreno, S. (2012). Fission yeast TORC1 prevents eIF2α phosphorylation in response to nitrogen and amino acids via Gcn2 kinase. J. Cell Sci**.** *125,* 5955-5959.
24. Reinders, A., Bürckert, N., Boller, T., Wiemken, A., and De Virgilio, C. (1998). *Saccharomyces cerevisiae* cAMP-dependent protein kinase controls entry into stationary phase through the Rim15p protein kinase. Genes Dev. *12,* 2943-2955.
25. Pedruzzi, I. Dubouloz, F., Cameroni, E., Wanke, V., Roosen, J., Winderickx, J., and De Virgilio, C. (2003). TOR and PKA signalling pathways converge on the protein kinase Rim15 to control entry into G0. Mol. Cell *12,* 1607-1613.
26. Wei, M., Fabrizio, P., Hu, J., Ge, H., Cheng, C., Li, L., and Longo, W. (2008). Life span extension by calorie restriction depends on Rim15 and transcription factors downstream of Ras/PKA, Tor, and Sch9. PLoS Genet. *4,* e13.
27. Sarkar, S., Dalgaard, J.Z., Millar, J.B., and Arumugam P. (2014). The Rim15-endosulfine-PP2ACdc55 signalling module regulates entry into gametogenesis and quiescence via distinct mechanisms in budding yeast. PLoS Genet. *10,* e1004456.

28. Bontron, S., Jaquenoud, M., Vaga, S., Talarek, N., Bodenmiller, B., Aebersold, R., and De Virgilio C. (2013). Yeast endosulfines control entry into quiescence and chronological life span by inhibiting protein phosphatase 2A. Cell Rep. *3,* 16-22.
29. Alvarez, B., and Moreno, S. (2006). Fission yeast Tor2 promotes cell growth and represses cell differentiation. J. Cell Sci. *119,* 4475-4485.
30. Urban, J., Soulard, A., Huber, A., Lippman, S., Mukhopadhyay, D., Deloche, O., Wanke, V., Anrather, D., Ammerer, G., Riezman, H., Broach, J.R., De Virgilio, C., Hall, M.N., and Loewith, R. (2007). Sch9 is a major target of TORC1 in *Saccharomyces cerevisiae*. Mol. Cell *26*, 663-674.
31. Rallis, C., López-Maury, L., Georgescu, T., Pancaldi, V., and Bähler, J. (2014). Systematic screen for mutants resistant to TORC1 inhibition in fission yeast reveals genes involved in cellular ageing and growth. Biol. Open *3*, 161-171.
32. Carpi, A., Krug, K., Graf, S., Koch, A., Popic, S., Hauf, S., and Macek, B. (2014). Absolute proteome and phosphoproteome dynamics during the cell cycle of fission yeast. Mol. Cell. Proteomics *13,* 192–1936.
33. Kettenbach, A.N., Deng, L., Wu, Y., Baldissard, S., Adamo, M.E., Gerber, S.A., and Moseley, J.B. (2015). Quantitative phosphoproteomics reveals pathways for coordination of cell growth and division by the conserved fission yeast kinase Pom1. Mol. Cell. Proteomics *14*, 1275-1287.
34. Pearce, L.R., Komander, D., and Alessi, D.R. The nuts and bolts of AGC protein kinases. Nat. Rev. Mol. Cell Biol. *11*, 9-22.
35. Juanes, M.A., Khoueiry, R., Kupka, T., Castro, A., Mudrak, I., Ogris, E., Lorca, T., and Piatti, S. (2013). Budding yeast greatwall and endosulfines control activity and spatial regulation of $PP2A^{Cdc55}$ for timely mitotic progression. PLoS Genet. *9,* e10033575.
36. Petersen, J., and Hagan, I.M. (2005). Polo kinase links the stress pathway to cell cycle control and tip growth in fission yeast. Nature *435,* 507-512.
37. Shiozaki, K., and Russell, P. (1995). Cell-cycle control linked to extracellular environment by MAP kinase pathway in fission yeast. Nature *378,* 739-743.
38. Millar, J.B., Buck, V., and Wilkinson, M.G. (1995). Pyp1 and Pyp2 PTPases dephosphorylate an osmosensing MAP kinase controlling cell size at division in fission yeast. Genes Dev. *9,* 2117-2130.
39. Martin, S.G., and Berthelot-Grosjean, M. (2009). Polar gradients of the DYRK-family kinase Pom1 couple cell length with the cell cycle. Nature *459,* 852-856.
40. Moseley, J.B, Mayeux, A., Paoletti, A., and Nurse, P. (2009). A spatial gradient coordinates cell size and mitotic entry in fission yeast. Nature *459,* 857-860.

41. Tyson, J.J., Csikasz-Nagy, A., and Novak, B. (2002). The dynamics of cell cycle regulation. Bioessays *24,* 1095-1109.
42. Clarke, P.R., Hoffmann, I., Draetta, G., and Karsenti, E. (1993). Dephosphorylation of cdc25-C by a type-2A protein phosphatase: specific regulation during the cell cycle in *Xenopus* egg extracts. Mol. Biol. Cell *4,* 397-411.
43. Mochida, S., Ikeo, S., Gannon, J., and Hunt, T. (2009). Regulated activity of PP2A-B55 delta is crucial for controlling entry into and exit from mitosis in *Xenopus* egg extracts. EMBO J. *28,* 2777-2785.
44. Gavet, O., and Pines, J. (2010). Progressive activation of CyclinB1-Cdk1 coordinates entry to mitosis. *Dev. Cell 18,* 533-543.
45. Moreno-Torres, M., Jaquenoud, M., and De Virgilio, C. (2015). TORC1 controls G1-S cell cycle transition in yeast via Mpk1 and the greatwall kinase pathway. Nature Comm. *6*, 8256.
46. Talarek, N., Cameroni, E., Jaquenoud,M., Luo, X., Bontron, S., Lippman, S., Devgan, G., Snyder, M., Broach, J.R., and De Virgilio, C. (2010). Initiation of the TORC1-regulated G0 program requires Igo1/2, which license specific mRNAs to evade degradation via the 5'-3' mRNA decay pathway. Mol. Cell *38,* 345-355.
47. Rossio, V., and Yoshida, S. (2011). Spatial regulation of Cdc55-PP2A by Zds1/Zds2 controls mitotic entry and mitotic exit in budding yeast. J. Cell Biol. *193,* 445-454.
48. Shima, H., Pende, M., Chen, Y., Fumagalli, S., Thomas, G., and Kozma, S.C. (1998). Disruption of the p70S6K/p86S6K gene reveals a small mouse phenotype and a new functional S6 kinase. EMBO J. *17,* 6649-6659.
49. Moreno, S., Klar, A., and Nurse, P. (1991). Molecular genetic analysis of fission yeast *Schizosaccharomyces pombe*. Methods Enzymol. *194,* 795-823.
50. Bähler, J., Wu, J.Q., Longtine, M.S., Shah, N.G., McKenzie, A. 3rd, Steever, A.B., Watch, A., Philippsen, P., and Pringle, J.R. (1998). Heterologous modules for efficient and versatile PCR-based gene targeting in *Schizosaccharomyces pombe*. Yeast *14,* 943-951.

Figure Legends

Figure 1. Igo1 and Ppk18 are required to advance entry into mitosis upon nutritional shift-down

(A-C) Wild-type and *igo1Δ* mutant cells grown in YES at 32ºC were shifted to minimal medium containing 20 mM glutamate (MMGlu) for 24 hours and then to minimal medium with 20 mM isoleucine (MMIle), or 20 mM phenylalanine (MMPhe) for another 24 hours at 32ºC.

(A) Images of exponentially growing cells stained with blankophor. Scale bar, 10 µm.

(B) Average cell length of 100 septated cells ± s.d. in YES, MMGlu and MMPhe.

(C) FACS profile of ethanol-fixed cells stained with propidium iodide. Wild-type (left), *igo1Δ* (right).

(D-F) Wild-type, *igo1Δ*, *cek1Δ*, *ppk18Δ* and *ppk18Δ cek1Δ* cells were grown in minimal medium containing 20 mM glutamate (MMGlu) and then shifted to minimal medium with 20 mM phenylalanine (MMPhe) at 32ºC.

(D) Images of exponentially growing cells in MMPhe stained with blankophor. Scale bar, 10 µm.

(E) Average cell length at division ± s.d. in MMGlu and MMPhe at 32ºC.

(F) FACS profile of the wild-type, *igo1Δ*, *cek1Δ*, *ppk18Δ* and *ppk18Δ cek1Δ* strains in MMPhe at 32ºC. Forward scatter (FSC), which correlates with cell size (left). DNA content (1C and 2C) after propidium iodide staining (right).

The numbers in the images indicate the average length of 100 septated cells ± the standard deviation (s.d.) (µm; n=100; means $p<0.001$ determined by independent samples t-test).

Figure 2. PP2A·B55 prevents entry into mitosis and acts downstream from Igo1

(A) Images of exponentially growing wild-type, *ppa1Δ* and *ppa2Δ* cells growing in YES at 32ºC stained with blankophor. Scale bar, 10 µm.

(B) Images of exponentially growing wild-type and *nmt1(41)-GST-pab1*$^{+}$ cells in YES at 32ºC stained with blankophor. Scale bar, 10 µm. YES is a rich medium that contains sufficient thiamine to represses the *nmt1* (version 41) promoter producing low levels of GST-Pab1.

(C) Images of wild-type and *nmt1(41)-GST-pab1⁺* cells exponentially growing in MMGlu (promoter derepressed, high levels of GST-Pab1) or in MMGlu+T (promoter repressed, low levels of GST-Pab1) at 32ºC stained with blankophor. Scale bar, 10 µm.

(D) Images of exponentially growing wild-type, *ppa2Δ*, *igo1Δ*, *ppa2Δ igo1Δ*, *igo1-S64A, ppa2Δigo1-S64A, nmt1(41):GST:pab1⁺*, and *nmt1(41):GST:pab1⁺ igo1Δ* cells growing on minimal medium with glutamate (MMGlu), except for *nmt1(41):GST:pab1⁺* and *mt1(41):GST:pab1⁺ igo1Δ* that were grown on MMGlu+T (promoter repressed, low levels of GST-Pab1), at 32ºC. Scale bar, 10 µm.

The numbers in the images indicate the average length of 100 septated cells ± the standard deviation (s.d.) (µm; n=100; means $p<0.001$ determined by independent samples t-test). See also Figure S1.

Figure 3. Ppk18 promotes entry into mitosis in an Igo1-dependent manner

Wild-type and mutant cells containing a copy of the *nmt1* promoter (version 41) integrated upstream from the *ppk18⁺* or *the cek1⁺* open reading frames (*nmt1(41):ppk18⁺, nmt1(41):cek1⁺*) in *igo1+* and *igo1Δ* mutant cells were grown in minimal medium containing 20 mM glutamate and 5 µM thiamine (MMGlu+T) to mid-exponential phase and then washed twice with MMGlu and incubated in the same medium without thiamine to induce the expression of *ppk18⁺* or *cek1⁺*.

(A) Images of exponentially growing cells stained with blankophor in the presence of thiamine (+ Thiamine, promoter OFF) or 20 hours after the removal of thiamine (- Thiamine, promoter ON). Scale bar, 10 µm. The numbers in the images indicate the average length of 100 septated cells ± the standard deviation (s.d.) (µm; n=100; means $p<0.001$ determined by independent samples t-test).

(B) FACS profile of ethanol-fixed cells stained with propidium iodide during the induction of *ppk18⁺* and *cek1⁺*. Wild-type cells were used as a control (left).

Figure 4. Ppk18–dependent *in vivo* phosphorylation of Igo1 at serine 64 upon nitrogen deprivation and starvation

(A) Representation of the Igo1 protein showing the highly conserved peptide sequence (boxed) around the serine 64 site of phosphorylation by greatwall. The sequences shown correspond to ARPP-19A and ARPP-19B from *Xenopus* (X), ARPP-19 from human

(H), ENSA from *Xenopus* (X) and from human (H), Igo1 and Igo2 from *S. cerevisiae* (Sc) and Igo1 from *S. pombe* (Sp).

(B) Levels of Igo1 and of Igo1 phosphorylated at Ser64 in *igo1Δ,* wild-type, *ppk18Δ*, *cek1Δ, ppk18Δ cek1Δ, ppk18-kinase dead (KD)* and *igo1-S64A* mutants in nitrogen-rich medium (MMGlu) and in nitrogen-poor medium (MMPhe). Tubulin was used as a protein loading control. See also Figure S4.

(C) Images of exponentially growing wild-type, *igo1Δ* and *igo1-S64A* cells in MMPhe stained with blankophor. Scale bar, 10 µm. The numbers in the images indicate the average length of 100 septated cells ± the standard deviation (s.d.) (µm; n=100; means $p<0.001$ determined by independent samples t-test).

(D) FACS profile showing the DNA content (1C and 2C) of wild-type, *igo1Δ* and *igo1-S64A* cells growing in MMGlu and MMPhe.

(E-I) Igo1 is rapidly phosphorylated at serine 64 upon nitrogen deprivation. Wild-type, *igo1Δ, igo1-S64A* and *ppk18Δ* mutant cells were grown in minimal medium with glutamate (MMGlu) at 32ºC and then shifted to minimal medium with phenylalanine (MMPhe) at the same temperature. Samples were collected at the indicated time-points for protein extracts, DAPI and blankophor staining and for FACS analysis.

(E) Levels of Igo1 and of Igo1 phosphorylated at Ser64 in the wild-type. Phosphorylation of eiF2α at Ser52 and of Rps6 (fission yeast ribosomal protein S6) at serines 235 and 236 were used as indicators of TOR activity. Tubulin was used as a protein loading control. There are two 0 time-points, one corresponding to cell extracts obtained from cells growing in MMGlu and the other corresponding to cell extracts obtained from cells immediately after the washes in MMPhe.

(F) Levels of Igo1 and of Igo1 phosphorylated at Ser64 in the wild-type and in the *ppk18Δ* mutant.

(G) Percentage of mitotic cells (two nuclei) in DAPI-stained ethanol-fixed cells (wild-type, closed circles, *igo1Δ*, open circles and igo1-S64A, open triangles).

(H) Percentage of septated cells in blankophor-stained ethanol-fixed cells (wild-type, closed circles, *igo1Δ*, open circles and *igo1-S64A*, open triangles).

(I) FACS profile (DNA content, 1C and 2C) of wild-type, *igo1Δ, igo1-S64A* and *ppk18Δ* ethanol-fixed cells stained with propidium iodide at different times after the shift from MMGlu to MMPhe.

(J,K) Wild-type, *ppk18Δ* and *igo1Δ* cells were grown in minimal medium with glutamate (MMGlu) at 25°C and then shifted to minimal medium without nitrogen (MM-N) at the same temperature. Samples were collected at the indicated time-points for protein extracts and FACS analysis (see Figure S2).

(J) Levels of Igo1 and of Igo1 phosphorylated at Ser64. Phosphorylation of Rps6 (fission yeast ribosomal protein S6) at Ser 235/236 was used to monitor TOR activity. Tubulin was used as a protein loading control.

(K) Mating efficiency of homothallic h^{90} wild-type, *h^{90} igo1Δ, h^{90} ppk18Δ, and h^{90} igo1-S64A* cells from 3 independent clones spotted onto sporulation medium (Malt extract plates). Cells overexpressing *tor2* (*h^{90} nmt1:tor2^{+}*) were used as a negative control for mating.

The numbers under the gels in 4B, 4E and 4J indicate the Igo1-P/Igo1 ratio (see Table S1).

Figure 5. Ppk18-dependent *in vivo* phosphorylation of Igo1 at serine 64 upon inactivation of TORC1

(A-B) Wild-type, *igo1Δ*, *tor2-51* and *tor2-51 ppk18Δ* cells were grown in rich YES medium at 25°C and then shifted to 35ºC. Samples were collected at the indicated time-points for protein extracts.

(A) Levels of Igo1 and of Igo1 phosphorylated at Ser64. Phosphorylation of Rps6 (fission yeast ribosomal protein S6) at Ser235/236 was used as an indicator of TOR activity and Tubulin as a protein loading control.

(B) Images of exponentially growing cells in YES at 35ºC stained with blankophor. The cell size of the *tor2-51 igo1Δ* double mutant was greater than the size of *tor2-51* and similar to that of *igo1Δ,* suggesting that Tor2 (TORC1) acts upstream from Igo1. Scale bar, 10 µm. The numbers in the images indicate the average length of 100 septated cells ± the standard deviation (s.d.) (µm; n=100; means $p<0.001$ determined by independent samples t-test).

(C-D) Down-regulation of TOR with Rapamycin or Torin activates the Ppk18-Igo1 pathway. Wild-type, *igo1Δ* and *ppk18Δ* cells were grown in rich YES medium at 25°C and then treated with Rapamycin or Torin. Samples were collected at the indicated time-points for protein extracts. DMSO was used as a control vehicle.

(C) Levels of Igo1 and of Igo1 phosphorylated at Ser64 after treatment with Rapamycin.
(D) Levels of Igo1 and of Igo1 phosphorylated at Ser64 after treatment with Torin. Extracts from cells lacking Igo1 (*igo1Δ*) or Ppk18 (*ppk18Δ*) were used to show the specificity of the Igo1 and Igo1-PS64 antibodies and the dependence of Igo1 phosphorylation on Ppk18, respectively. Phosphorylation of Rps6 (fission yeast ribosomal protein S6) at Ser235/236 was used as an indicator of TOR activity and Tubulin as a protein loading control.
The numbers under the gels in 5A, 5C and 5D indicate the Igo1-P/Igo1 ratio (see Table S1).

Figure 6. Sck2 negatively regulates the Ppk18-Igo1 pathway
(A) Average cell length at division ± s.d. of wild-type, *nmt1:sck1*$^{+}$, *nmt1:sck2*$^{+}$ and *nmt1:psk1*$^{+}$ cells growing in nitrogen-rich medium (MM+NH_4Cl) at 32ºC in the presence (+T, promoter OFF) or 20 hours after the removal of thiamine (-T, promoter ON).
(B) Levels of Igo1 and Igo1 phosphorylated at Ser64 in wild-type, *nmt1:sck1*$^{+}$, *nmt1:sck2*$^{+}$ and *nmt1:psk1*$^{+}$ growing in nitrogen-poor medium (MMPhe) at 32ºC in the presence (+T, promoter OFF) or in the absence of thiamine (-T, promoter ON). See also Figure S3.
(C) Images of exponentially growing wild-type, *ppk18-2A*^{S6K}, *ppk18-4A*$^{PKA/S6K}$ and *ppk18-6A*$^{PKA/S6K}$ mutants growing in nitrogen-rich medium (MM+NH_4Cl) at 32ºC stained with blankophor. Scale bar, 10 µm. The numbers in the images indicate the average length of 100 septated cells ± the standard deviation (s.d.) (µm; n=100; means $p<0.001$ determined by independent samples t-test).
(D) Levels of Igo1 and of Igo1 phosphorylated at Ser64 in wild-type, *ppk18-2A*^{S6K}, *ppk18-4A*$^{PKA/S6K}$ and *ppk18-6A*$^{PKA/S6K}$ mutant cells growing in nitrogen-rich medium (MM+NH_4Cl) at 32ºC. The numbers indicate the Igo1-P/Igo1 ratio (see Table S1). Tubulin was used as a protein loading control.

Figure 7. Mathematical model for nutritional control of mitosis in fission yeast
(A) Nutrient availability regulates Cdk1 auto-activation at the G2/M transition through kinases TOR and greatwall, Igo1-P and PP2A. Activation of greatwall by Cdk1 renders PP2A and Cdk1 mutually inhibitory.

(B-D) Steady-states of Cdk1 activity (low, intermediate and high) are plotted as a function of cell size for wild-type in rich (B) and poor media (D) as well as for the *igo1Δ* mutant (C) in both rich and poor media. The blue curve shows the fluctuation of Cdk1 activity in rich medium for wild type (B and D) and *igo1Δ* cells (C). Wild-type cells are shifted from rich to poor medium (arrow) at three different times and at three different sizes (pink, orange and red curves) in G2. In each case, the shifted cell activates Cdk1 almost immediately and enters into mitosis at a small size (D). See also Figure S5.

Figure 1

Click here to download Figure Figure 1.tif

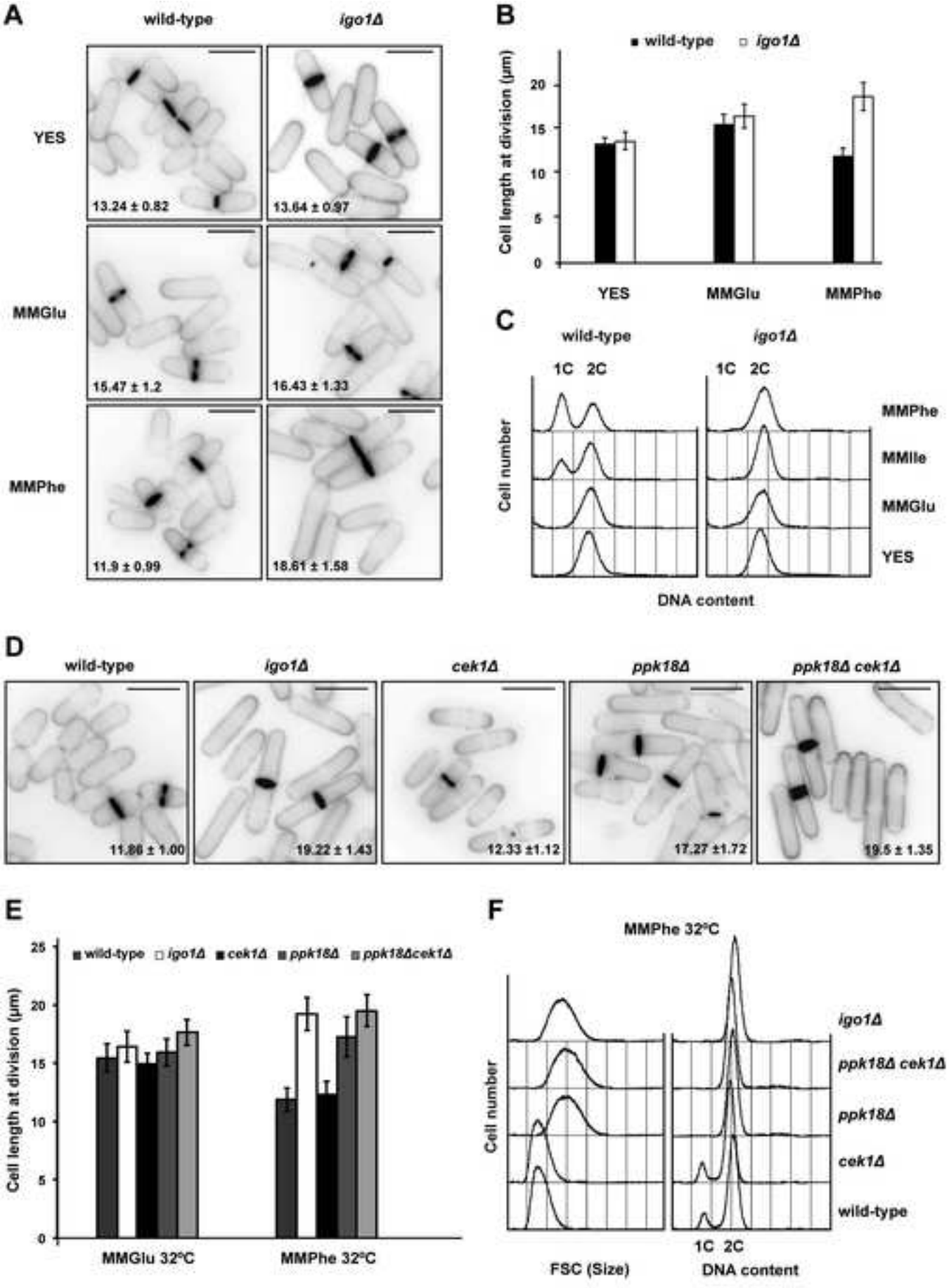

Figure 1 (Moreno)

Figure 2

Click here to download Figure Figure 2.tif

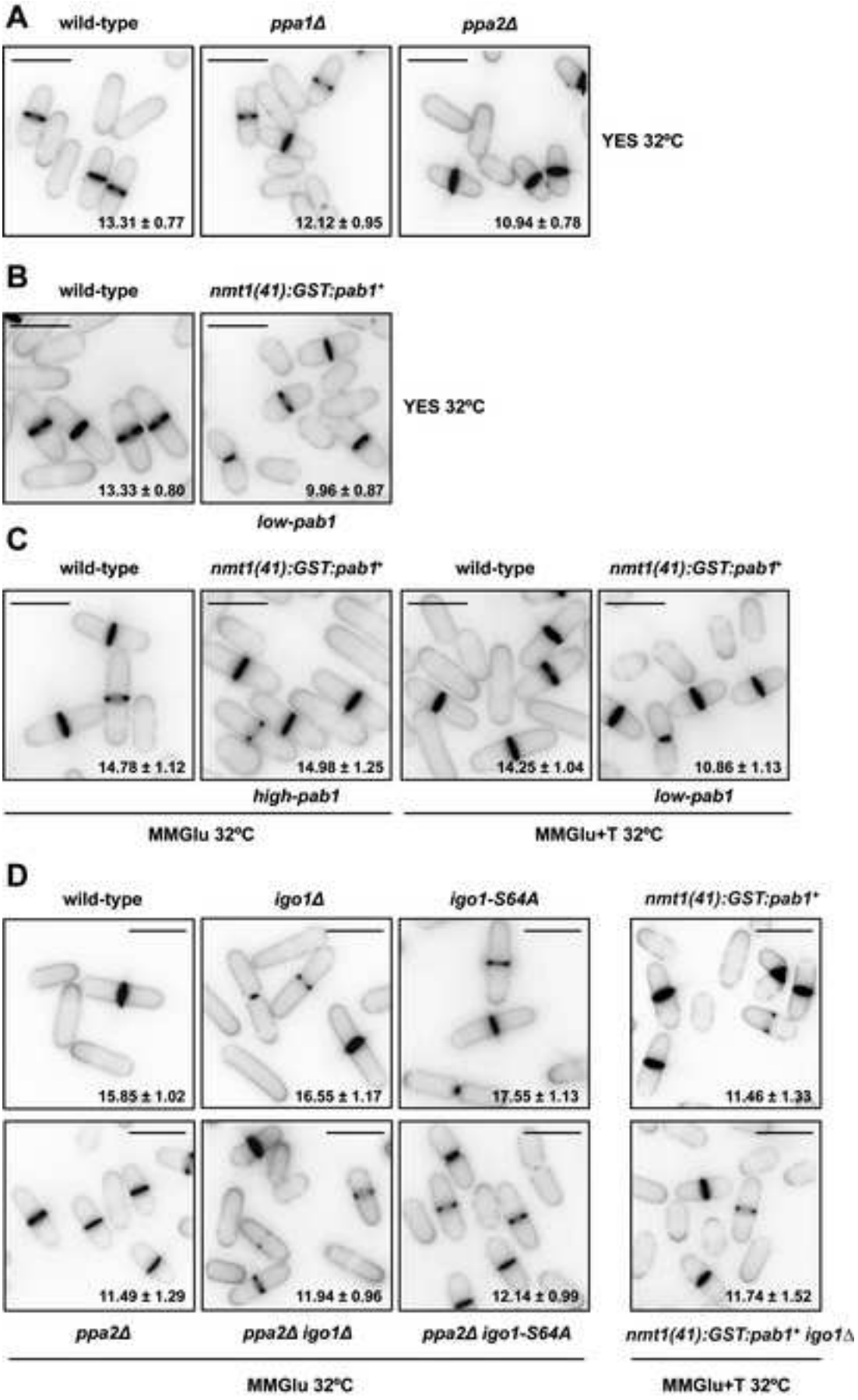

Figure 2 (Moreno)

Figure 3

Click here to download Figure Figure 3.tif

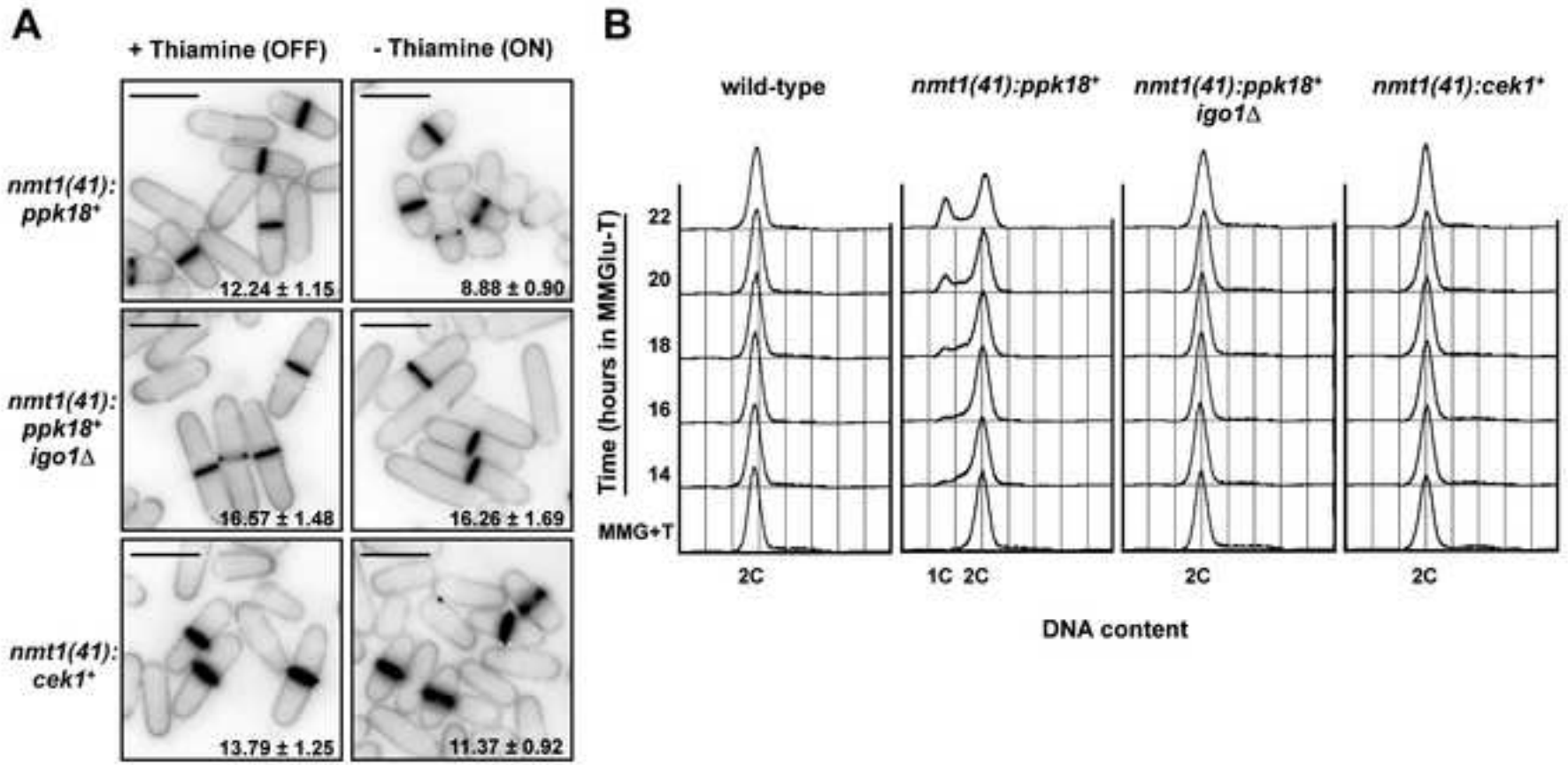

Figure 3 (Moreno)

Figure 4

Click here to download Figure Figure 4.tif

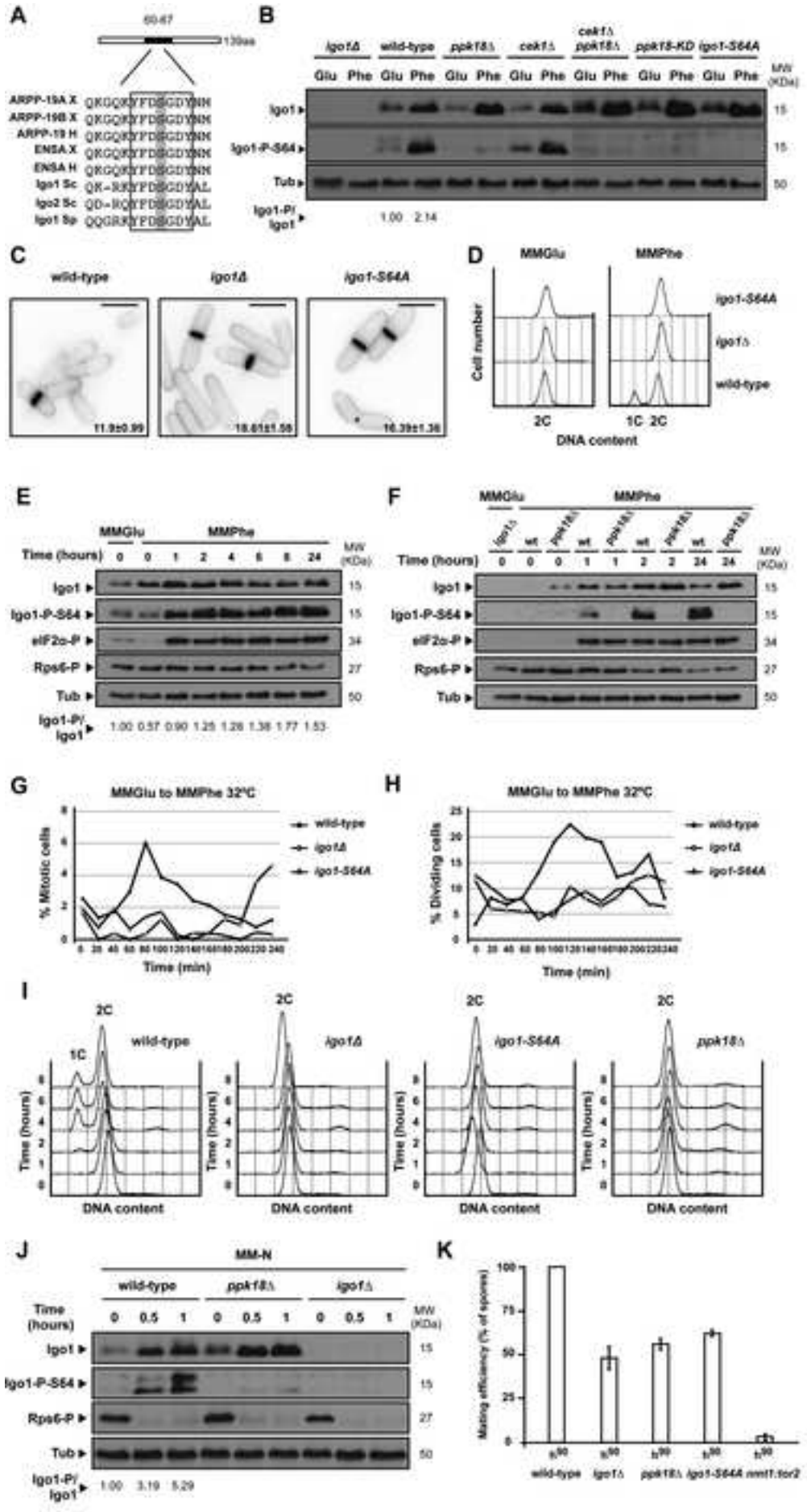

Figure 4 (Moreno)

Figure 5

Click here to download Figure Figure 5.tif

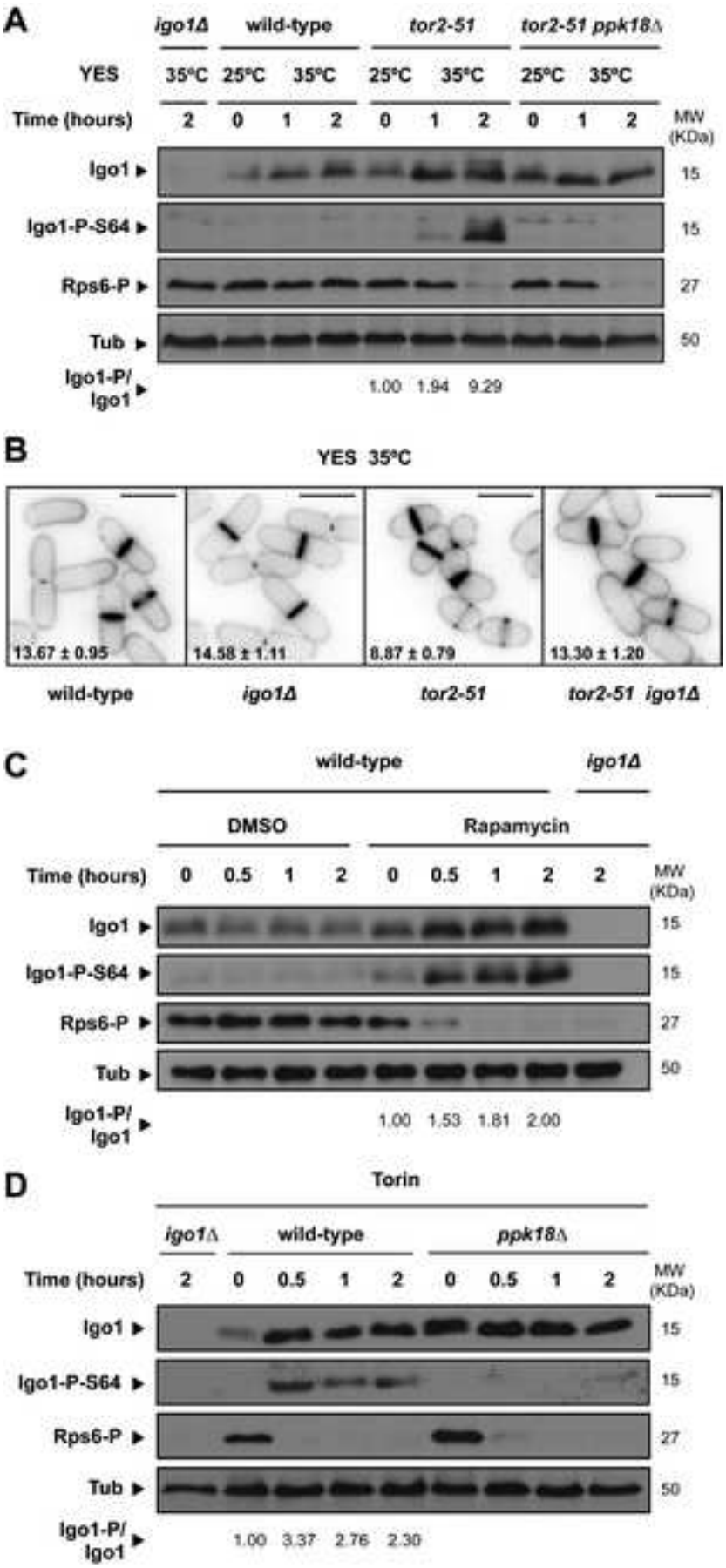

Figure 5 (Moreno)

Figure 6

Click here to download Figure Figure 6.tif

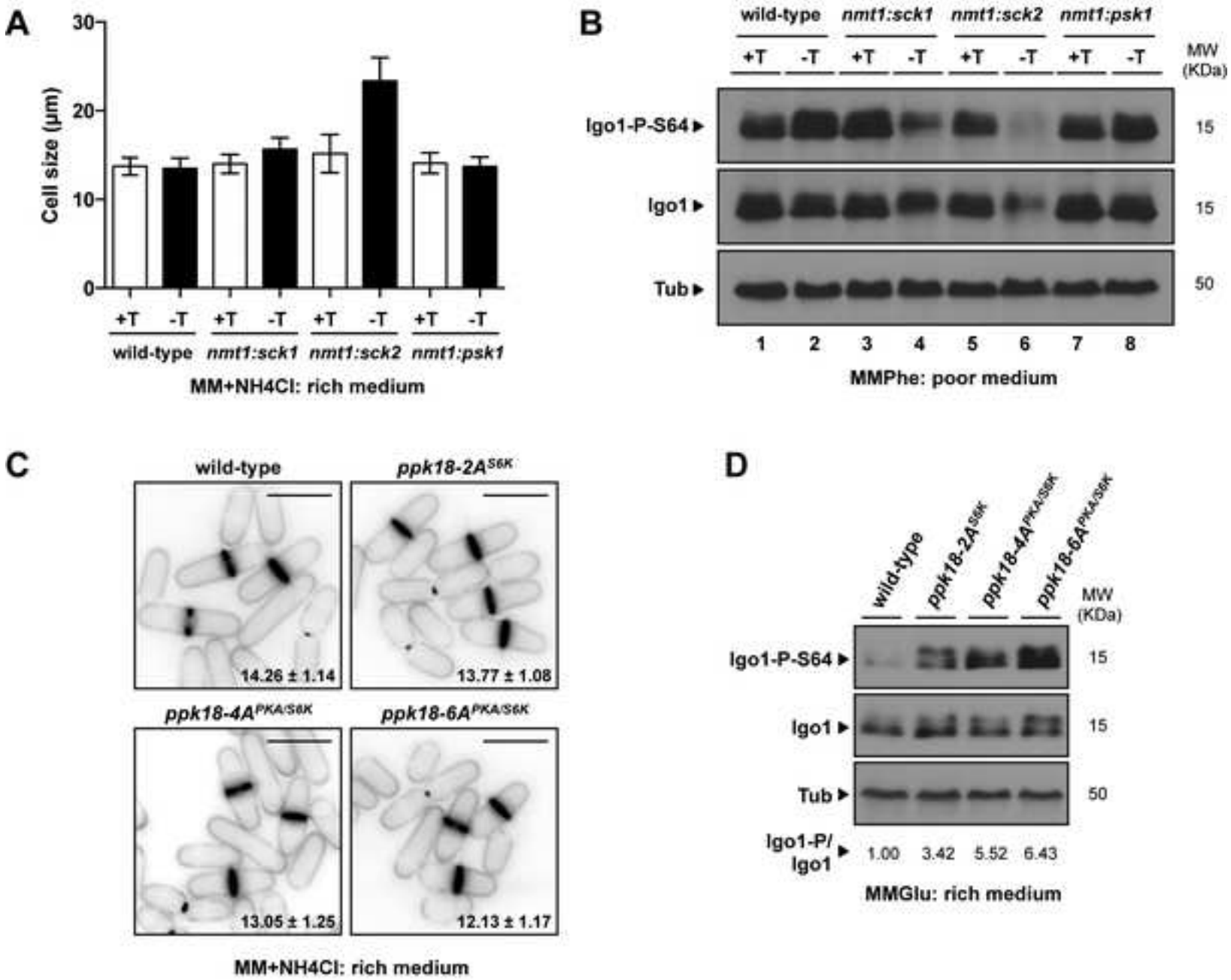

Figure 6 (Moreno)

Figure 7

Click here to download Figure Figure 7.tif

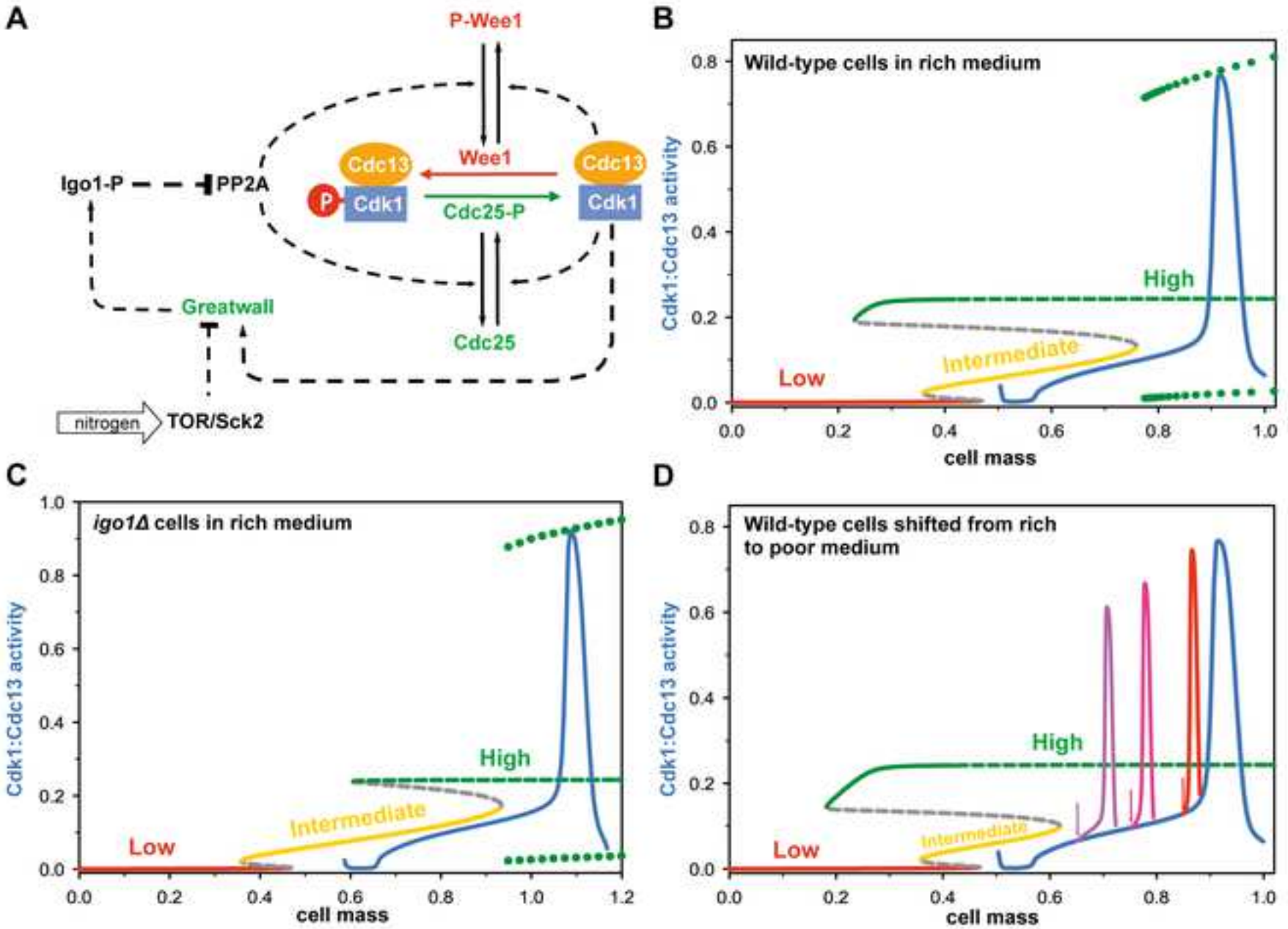

Figure 7 (Moreno)

Supplemental Information

Nutritional control of cell size by the greatwall-endosulfine-PP2A·B55 pathway

Nathalia Chica, Ana Elisa Rozalén, Livia Pérez-Hidalgo, Angela Rubio, Bela Novak and Sergio Moreno

Inventory of Supplemental Information

Supplemental Information includes 5 supplemental figures, 2 supplemental movies, 2 supplemental tables, supplemental experimental procedures, mathematical model and code and supplemental references.

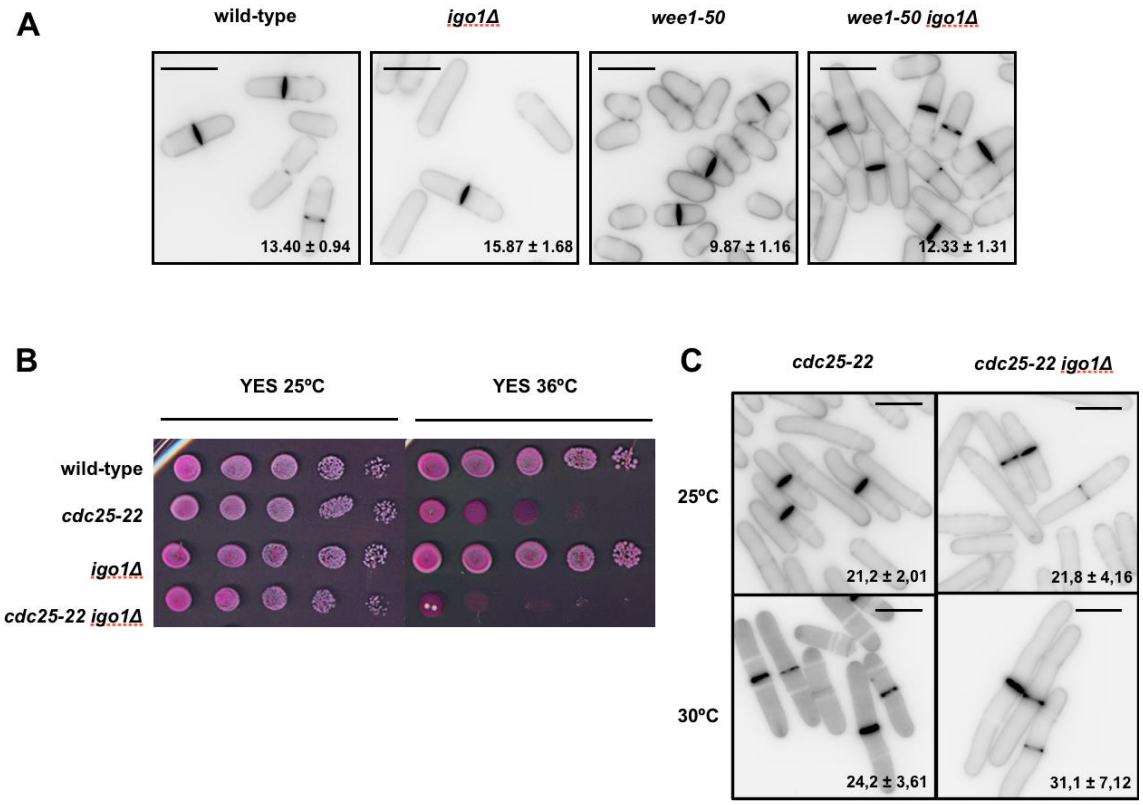

Figure S1 (related to Figure 2). *igo1Δ* mutant suppresses the reduced cell size of *wee1-50* and enhances the temperature sensitive and elongated phenotype of *cdc25-22*

(A) Images of exponentially growing wild-type, *igo1Δ, wee1-50* and *wee1-50 igo1Δ* in MMGlu at 25ºC stained with blankophor. Scale bar, 10 µm. (B) Spot assay of mid-exponential phase cultures of wild-type, *cdc25-22*, *igo1Δ* and *cdc25-22 igo1Δ* cell mutants on YES with Phloxin B at 25ºC and 36ºC and imaged after 48h. (C) Images of exponentially growing *cdc25-22* and *cdc25-22 igo1Δ* cells in YES at 25ºC and 30ºC stained with blankophor. Scale bar, 10 µm.

The numbers in the images indicate the average length of 100 septated cells ± the standard deviation (s.d.) (µm; n=100; means $p<0.001$ determined by independent samples t-test).

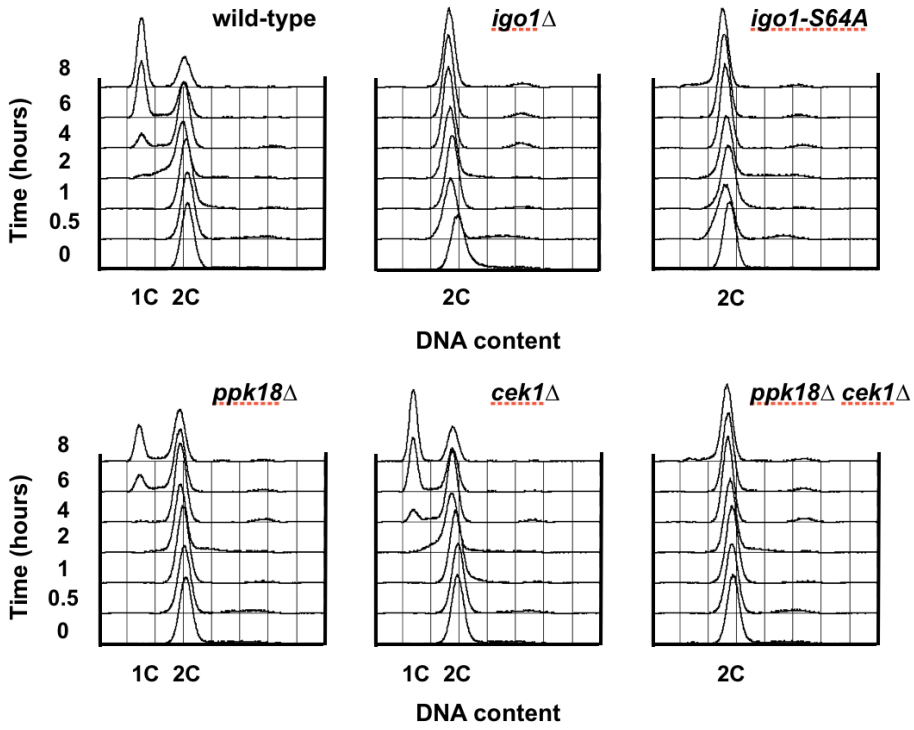

Figure S2 (related to Figure 4J). Fission yeast greatwall and endosulfine are required for G1 arrest upon nitrogen starvation.

FACS profiles (DNA content, 1C and 2C) of ethanol-fixed cells stained with propidium iodide of the wild-type, *igo1Δ, igo1-S64A, ppk18Δ, cek1Δ* and *ppk18Δ cek1Δ* cells grown in minimal medium with glutamate (MMGlu) at 25°C and then shifted to minimal medium without nitrogen (MM-N) at the same temperature. Samples were collected at the indicated time-points after the shift.

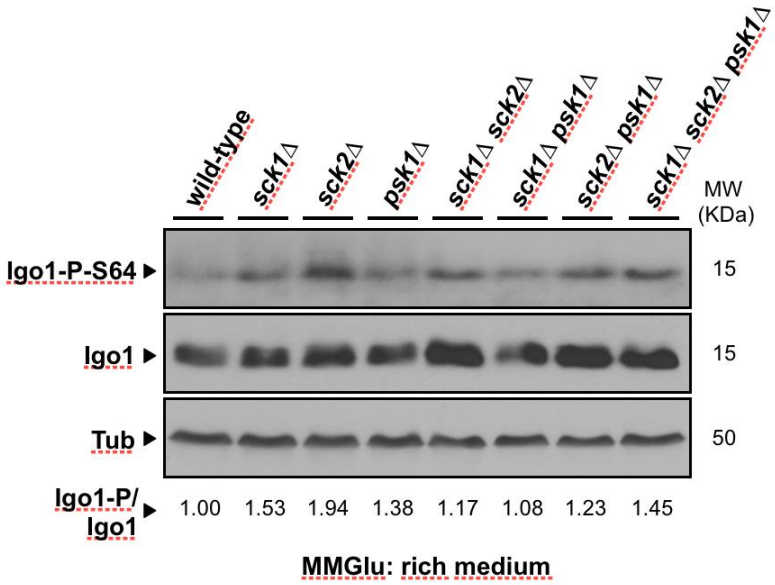

Figure S3 (related to Figure 6B). Phosphorylation of Igo1 at Ser64 in S6-kinase mutants.

Levels of Igo1 and Igo1 phosphorylated at Ser64 in wild-type, *sck1Δ*, *sck2Δ*, *psk1Δ*, *sck1Δ sck2Δ*, *sck1Δ psk1Δ*, *sck2Δ psk1Δ*, and *sck1Δ sck2Δ psk1Δ* in nitrogen-rich medium (MMGlu). The numbers indicate the Igo1-P/Igo1 ratio (see Table S1). Tubulin was used as a protein loading control.

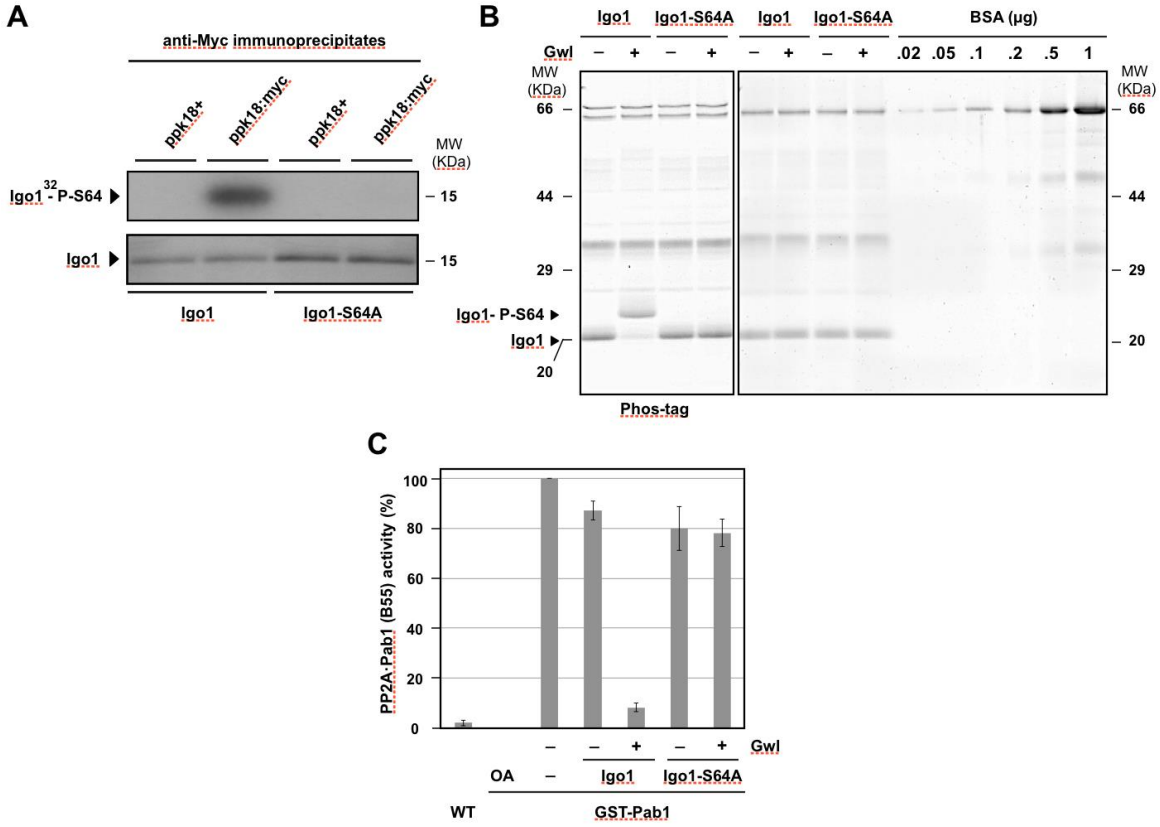

Figure S4 (related to Figure 4B). Ppk18 phosphorylates Igo1 at Ser64 and phosphorylated Igo1 inhibits PP2A·Pab1.

A) Extracts from the wild-type (*ppk18+*) cells and from cells expressing Ppk18-13myc, treated for 1 hour with rapamycin, were immunoprecipitated with anti-c-Myc antibodies. Kinase assays of the Ppk18-13myc immunoprecipitates using purified recombinant Igo1 and Igo1-S64A in the presence of γ-^{32}P-ATP (top). Coomasie blue staining of the gel (bottom).

B) *In vitro* thio-phosphorylation reactions of purified recombinant wild-type Igo1 and Igo1-S64A mutant using *Xenopus* Greatwall. Left, 15% polyacrylamide Phos-tag gel. Right, standard 17% polyacrylamide gel of the same samples after centrifugation through Sephadex G-25 spin columns. Different amounts of BSA were run on the same gel to determine the concentration of the Igo1 and Igo1-S64A proteins.

C) *In vitro* inhibition of PP2A·Pab1 (B55) by thio-phosphorylated Igo1 (Igo1-P). PP2A·Pab1 phosphatase complex was purified from extracts of cells expressing GST-Pab1 using Glutathione-Sepharose beads. A wild-type extract was treated under identical conditions and used as a negative control (WT). PP2A·Pab1 phosphatase activity was determined in the absence and in the presence of thio-phosphorylated Igo1 or Igo1-S64A. OA, okadaic acid was used as a positive control. Each bar represents the mean ± the standard deviation (s.d.) of three independent experiments (p<0.05 determined using Student´s t-test).

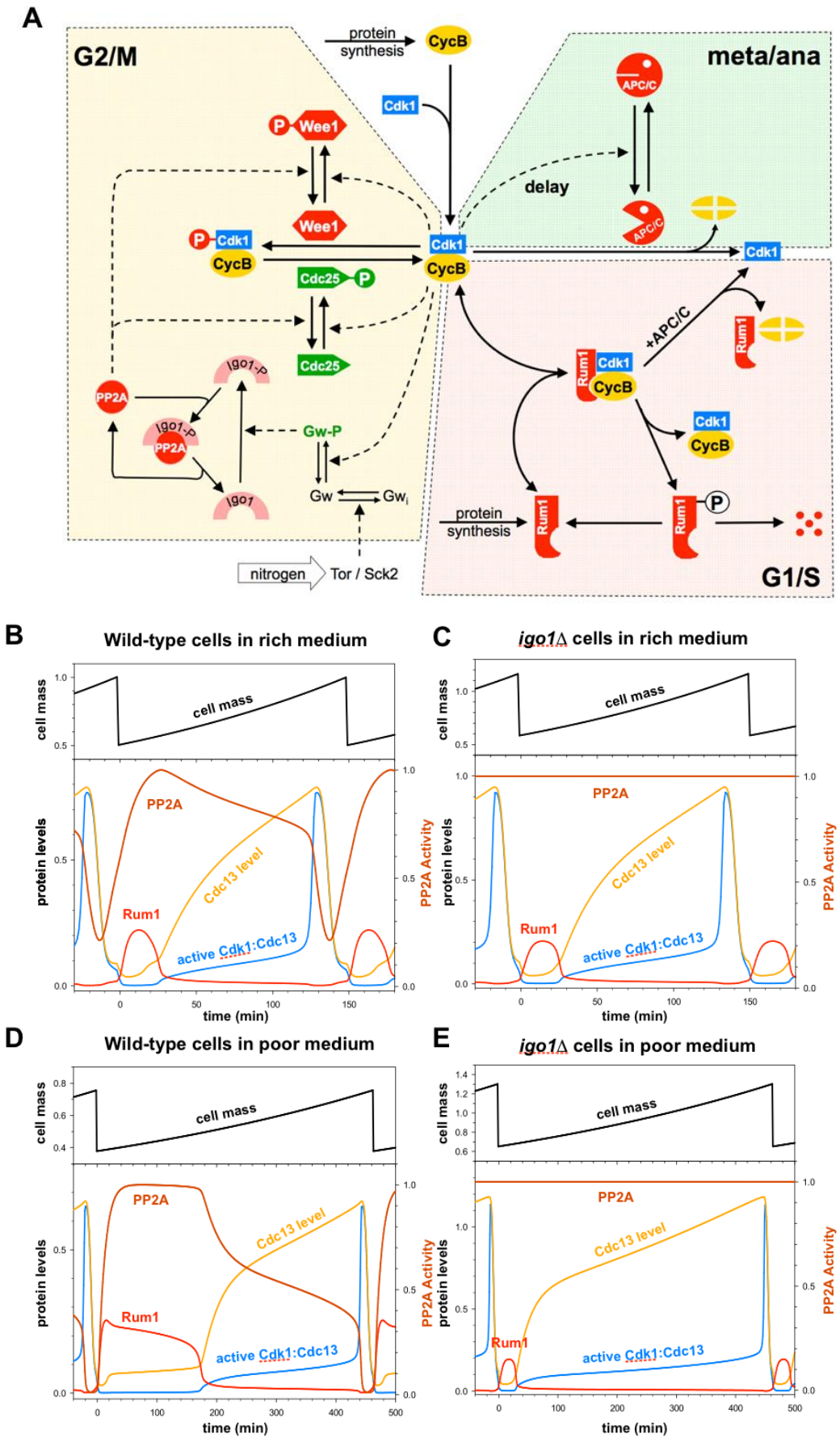
A
G2/M
meta/ana
G1/S
protein synthesis
CycB
Cdk1
Wee1
P
delay
APC/C
Cdc25
Igo1-P
PP2A
Gw-P
Gw
Gw$_i$
+APC/C
Rum1
nitrogen
Tor / Sck2
B
Wild-type cells in rich medium
C
igo1Δ cells in rich medium
D
Wild-type cells in poor medium
E
igo1Δ cells in poor medium
cell mass
protein levels
PP2A Activity
PP2A
Cdc13 level
Rum1
active Cdk1:Cdc13
time (min)

Figure S5 (related to Figure 7). Mathematical Model for nutritional control of mitosis in fission yeast

(A) The fission yeast cell cycle control network. Solid lines represent biochemical reactions, while dashed lines illustrate catalytic effects. Three different modules are responsible for the regulation of the Cdk1:CycB (Cdk1:Cdc13) complex. The reversible association with Cdk1 inhibitor Rum1 controls the G1/S transition. Phosphorylation and dephosphorylation by the inhibitory kinase Wee1 and the activating phosphatase Cdc25 regulates the G2/M transition. Cdk1:Cdc13 inhibits Rum1 and Wee1, while it activates Cdc25. These regulatory interactions create mutual inhibitions between Cdk1 and Rum1 and between Cdk1 and Wee1, and a mutual activation loop between MPF and Cdc25. The third module, responsible for meta/anaphase transition during mitosis, is based on a delayed negative feedback loop involving APC/C (Anaphase Promoting Complex/Cyclosome). This negative feedback loop, which causes the destruction of Cdc13 at the end of mitosis, is critical to generating sustained oscillations in Cdk1 activity. The "time delay" in the Figure is implemented in the differential equations by an Intermediary Enzyme (IE) between Cdk1 and APC/C.

(B-E) Numerical simulations of the fission yeast cell cycle in rich (B and C) and poor media (D and E). Wild-type (B and D) and *igo1*Δ mutant (C and E) cells.

Table S1. Quantification of Igo1-P and total Igo1 proteins in western blots

Figure 4B wild type	**MMG**	**MMF**
Igo1-P/Tub	1.00	3.71
Igo1/Tub	1.00	1.73
Ratio Igo1-P/Igo1	1.00	2.14

Figure 4E wild type in MMF	**MMG**	**Time in MMF (hours)**						
		0	**1**	**2**	**4**	**6**	**8**	**24**
Igo1-P/Tub	1.00	0.93	1.66	2.44	2.14	1.82	2.47	2.45
Igo1/Tub	1.00	1.63	1.85	1.95	1.68	1.32	1.40	1.60
Ratio Igo1-P/Igo1	1.00	0.57	0.90	1.25	1.28	1.38	1.77	1.53

Figure 4J wild type w/o Nitrogen	**Time in MM-N (hours)**		
	0	**0.5**	**1**
Igo1-P/Tub	1.00	7.78	16.84
Igo1/Tub	1.00	2.44	3.19
Ratio Igo1-P/Igo1	1.00	3.19	5.29

Figure 5A *tor2-51*	**Time at 35ºC (hours)**		
	0	**1**	**2**
Igo1-P/Tub	1.00	3.13	16.86
Igo1/Tub	1.00	1.61	1.81
Ratio Igo1-P/Igo1	1.00	1.94	9.29

Figure 5C wild type + rapamycin	**Time in rapamycin (hours)**			
	0	**0.5**	**1**	**2**
Igo1-P/Tub	1.00	2.20	2.69	3.05
Igo1/Tub	1.00	1.43	1.49	1.52
Ratio Igo1-P/Igo1	1.00	1.53	1.81	2.00

Figure 5D wild type + torin	**Time in torin (hours)**			
	0	**0.5**	**1**	**2**
Igo1-P/Tub	1.00	9.61	5.68	5.82
Igo1/Tub	1.00	2.86	2.06	2.53
Ratio Igo1-P/Igo1	1.00	3.37	2.76	2.30

Figure 6D	**wild type**	***ppk18-2A***	***ppk18-4A***	***ppk18-6A***
Igo1-P/Tub	1.00	4.44	6.28	9.53
Igo1/Tub	1.00	1.30	1.14	1.48
Ratio Igo1-P/Igo1	1.00	3.42	5.52	6.43

Figure S3	**wt**	***sck1***	***sck2***	***psk1***	***sck1 sck2***	***sck1 psk1***	***sck2 psk1***	***sck1 sck2 psk1***
Igo1-P/Tub	1.00	1.70	2.66	1.54	2.19	1.42	2.39	2.16
Igo1/Tub	1.00	1.11	1.37	1.12	1.87	1.31	1.93	1.49
Ratio Igo1-P/Igo1	1.00	1.53	1.94	1.38	1.17	1.08	1.23	1.45

The intensity of the bands was quantified by densitometry using Image J (National Institutes of Health). The values of phosphorylated and total Igo1 protein were normalised to the levels of tubulin and given a value of 1 to the initial or control condition (MMG, 'time 0' or wild type). The phosphorylated fraction was expressed as the ratio of Igo1-phospho/Igo1 total protein.

Table S2. Epistatic analysis between *igo1Δ* and other mitotic regulators in MMGlu and MMPhe

Strain	Cell length in MMGlu (µm ± s.d.)	*p*-value	Cell lenght in MMPhe (µm ± s.d.)	*p*-value	Genetic Interaction
Wild-type	15.46 ± 1.12	---	11.9 ± 0.99	---	----
igo1Δ	16.43 ± 1.33	---	18.61 ± 1.58	---	---
cdr1Δ	17.33 ±1.12	10^{-12}	16.88 ±1.54	10^{-19}	---
cdr1Δ igo1Δ	18.75 ± 1.3	10^{-32}	20.62 ± 1,38	10^{-26}	Additive in MMGlu and MMPhe
pom1Δ	12.95 ±1.52	10^{-41}	10.19 ± 1.25	10^{-84}	---
pom1Δ igo1Δ	14.42 ±1.94	10^{-17}	13.68 ± 1.29	10^{--61}	Additive in MMGlu and MMPhe
pyp2Δ	14.63 ±1.3	10^{-25}	13.34 ± 1.3	10^{-63}	---
pyp2Δ igo1Δ	16.99 ±1.27	10^{-5}	17.1 ± 1.8	10^{-13}	Additive in MMPhe
sty1Δ	22.74 ±1.39	10^{-67}	Inviable	---	---
sty1Δ igo1Δ	26.59 ±2.29	10^{-68}	Inviable	---	Additive in MMGlu and MMPhe

Cell length represents the average length (in µm) of 100 septated cells ± the standard deviation. The *p*-value was calculated by the Student´s T test for a sample between the length of *igo1Δ* and the length of each mutant analysed. The level of significance used was $1x10^{-5}$.

Supplementary Experimental Procedures

Fission yeast strains

Strain	Genotype	Source
S2333	*h⁻ igo1::kanMX6*	This work
S2334	*h⁺ cdc25-22 igo1::kanMX6*	This work
S2335	*h⁻ cdc25-22*	P. Nurse
S2336	*h⁺ wee1-50 igo1::kanMX6*	This work
S2337	*h⁺ ppa2::natMX6*	This work
S2338	*h⁺ igo1::kanMX6 ppa2::natMX6*	This work
S2339	*h⁻ igo1::ura4⁺*	This work
S2341	*h⁻ ppk18::kanMX6*	This work
S2460	*h⁺ ppk18:: ura4⁺ ura4-D18 leu1-32 ade6-M210*	This work
S2342	*h⁺ tor2-51:ura4⁺*	S. Moreno
S2343	*h⁻ tor2-51:ura4⁺ ura4-D18 igo1::kanMX6*	This work
S2439	*h⁻ tor2-51:ura4⁺ ura4-D18 ppk18::kanMX6*	This work
S2344	*h⁻ igo1::natMX6*	This work
S2346	*h⁻ igo1::natMX6 ppk18::kanMX6*	This work
S2347	*h⁻ pka1::ura4⁺ ura4-D18*	M. Yamamoto
S2350	*h⁺ igo1:igo1-S64A*	This work
S2351	*h⁺ wee1-50 ppa2::natMX6*	This work
S2352	*h⁺ cdc25-22 ppa2::natMX6*	This work
S2354	*h⁻ igo1::kanMX6 pom1::ura4⁺ ura4-D18*	This work
S2355	*h⁻ igo1::kanMX6 pyp2::ura4⁺ ura4-D18*	This work
S2356	*h⁺ pyp2::ura4⁺ ura4D-18*	K. Shiozaki
S2357	*h⁻ igo1::kanMX6 sty1::ura4⁺ ura4-D18*	This work
S2358	*h⁻ sty1(spc1)::ura4⁺ ura4-D18*	K. Shiozaki
S2359	*h⁻ igo1::kanMX6 cdr1::natMX6*	This work
S2360	*h⁺ cek1::ura4+ ura4D-18*	This work
S2361	*h⁺ cek1::ura4+ ppk18::kanMX6 ura4-D18*	This work

S2368	*h+ ppk18::KanMX6*	This work
S817	*h- pom1::ura4+ ura4-D18*	P. Nurse
S999	*h+ wee1-50*	P. Nurse
S1000	*h- wee1-50*	P. Nurse
S2201	*h- 972*	P. Nurse
S2267	*h+ cdr1::natMX6*	P. Nurse
S2308	*h- ppa1::kanMX6*	This work
S2309	*h+ aur-mcherry:atb2 hht2:GFP:ura4+ ura4d-18*	M. Tormos
S2365	*h+ aur-mcherry:atb2 hht2:GFP:ura4+ ura4d-18 igo1::kanMX6*	This work
S2392	*h- kanMX6:nmt1(41X):GFP-ppk18*	This work
S2393	*h- kanMX6:nmt1(41X):GFP-ppk18 igo1::NatMX6*	This work
S2400	*h+ igo1:igo1-S64A ppa2::NatMX6*	This work
S2402	*h- ppk18-13myc:kanMX6*	This work
S2403	*h- kanMX6:nmt1(41):GST-pab1*	This work
S2431	*h+ kanMX6:nmt1(41):GST-pab1*	This work
S2432	*h+ kanMX6:nmt1(41):GST-pab1 igo1::KanMX6*	This work
S2049	*h90 968*	P. Nurse
S2313	*h90 igo1::KanMX6*	This work
S2430	*h90 igo1:igo1-S64A*	This work
S2447	*h90 ppk18::KanMX6*	This work
S2446	*h90 nmt1: tor2+*	S. Moreno
S2436	*h+ nmt1(41): cek1+*	S. Moreno
S2448	*h- ppk18-K595A (ppk18-KD)*	This work
S2449	*h- ppk18-2A*	This work
S2450	*h- ppk18-4A*	This work
S2451	*h- ppk18-6A*	This work
S2453	*h- sck1::kanMX6*	Bioneer
S2389	*h- sck2::natMX6*	C. Rallis
S2455	*h- psk1::kanMX6*	Bioneer
S2637	*h- sck1::KanMX6 sck2::natMX6*	This work

S2638	*h⁻ sck1::kanMX6 psk1::kanMX6*	This work
S2639	*h⁻ sck2::natMX6 psk1::kanMX6*	This work
S2640	*h⁻ sck1::KanMX6 sck2::natMX6 psk1::kanMX6*	This work
S2456	*h⁻ nmt1: sck1⁺*	This work
S2457	*h⁻ nmt1: sck2⁺*	This work
S2458	*h⁻ nmt1: psk1⁺*	This work

Mating assays

Serial dilutions of three independent clones of homothallic h^{90} wild-type, h^{90} *igo1Δ*, h^{90} *ppk18Δ*, h^{90} *igo1-S64A* and h^{90} *nmt1-tor2⁺* grown in YES were spotted onto sporulation medium (malt extract plates) and incubated for 48 hours at 25ºC. The cells were resuspended in water to a concentration of $3x10^6$ cells/ml and treated with glusulase (Sigma) for 14 hours to kill vegetative cells. The number of spores was determined by plating the same volume in yeast extract (YES) medium and counting the number of colonies generated after 72ºC at 25ºC.

Time lapse imaging and videos

Time-lapse imaging was performed in MMPhe, using an imaging chamber pre-treated with 10 mg/ml lectin (L1395; Sigma-Aldrich) and filled with 300 µl of exponentially growing wild-type (strain S2309) or *igo1Δ* (strain S2365) cells expressing mcherry-Atb2 and Hht2-GFP. After 3 minutes, cells were washed twice with MMPhe. Immediately after this, cells were examined using an Olympus Spinning Disk Confocal microscope equipped with a FRAP module, a 60x/1,42 A/N oil objective lens and a Photometrics Evolve camera. For time-lapse series, 7 Z-sections (0.5 µm step size) were taken every 2 minutes for 2 hours at 32ºC and maximum intensity projection was generated using MetaMorph software (Molecular Devices). Time-lapse videos were created and analysed using ImageJ (National Institutes of Health).

FACS analysis

Samples of 10^6 cells fixed in 70% (v/v) ethanol were washed with 1 ml of 50 mM sodium citrate and resuspended in 0.5 ml of 50 mM sodium citrate containing 0.1 mg/ml RNase A and incubated at 37°C overnight. Then, 0.5 ml of 50 mM sodium citrate containing 4 µg/ml propidium iodide was added and the samples were sonicated before analysis in a BD FACSCalibur instrument. Analysis was performed using BD Cell Quest Pro TM 6.0.3 (Biosciences).

Protein methods

Antibodies against Igo1 were prepared by injecting the Igo1 C-terminal peptide (C-GASSRRESVTRHDLE) coupled to KHL into rabbits [S1]. 12 ml of serum obtained after the 6^{th} injection were affinity-purified in a column containing the peptide coupled to CrBN-activated Sepharose 4B [S1] (Amersham Pharmacia Biotech). For the Igo1-serine 64 phospho-specific antibody, two peptides were synthesised, one containing phospho-serine 64 (C-GRKYFD**Sp**GDYALNK) and another one lacking the phosphate. This second peptide was used to deplete the antibodies that recognise Igo1 from the serum prior to the affinity purification with the phosphorylated peptide. Protein extracts were obtained using trichloroacetic acid

(TCA) extraction [S2]. For Western blots, 45 µg of total protein extract were run on 15% SDS-PAGE, transferred to PVDF Immobilon P membranes (Millipore), and probed with rabbit affinity-purified anti-Igo1 (1:200), anti-P-Ser64-Igo1 (1:100), rabbit anti-phospho-eIF2α (Ser51) (1:1000) (Cell Signaling Technology), for the phosphorylation of Rps6 rabbit anti-phospho-(Ser/Thr) Akt Substrate (1:1000) (Cell Signaling Technology), and mouse anti-tubulin (1:3000) (a gift from Dr. Keith Gull, Sir William Dunn School of Pathology, University of Oxford, UK) primary antibodies and, as secondary antibodies, NA 931 (anti-mouse IgG) or NA 934 (anti-rabbit), Horseradish Peroxidase (Amersham). Immunoblots were developed using the enhanced chemiluminescence procedure (ECL kit, Amersham and Advansta).

Igo1 purification and Ppk18 kinase assays

The *igo1*$^{+}$ cDNA was amplified from the Edgar and Norbury *S. pombe* cDNA library and cloned into the pET-15b vector. The *igo1-S64A* mutant was generated by site-directed mutagenesis using the pET-15b-*igo1* plasmid as a template and the Quikchange XL mutagenesis kit (Agilent). Igo1 and Igo1-S64A mutant proteins N-terminally tagged with 6xHis, were expressed and purified from *E. coli*. Briefly, 300 ml of bacteria cultures were grown in LB with ampicillin at 37ºC to an OD_{600nm} of 0.4. IPTG (isopropyl ß-D-1-thiogalactopyranoside) was added to a final concentration of 0.4 mM, and the cells were incubated at 16ºC for 16 hours. The bacteria cells were harvested by centrifugation, resuspended in 20 ml of binding buffer (20 mM Tris-HCl pH 7.9, 5 mM imidazole, 500 mM NaCl) with 0.1% Triton X-100, and frozen at -80ºC. Bacterial pellets were thawed, lysed by sonication (six cycles at 40% amplitude, 50 s on, 10 s off, on ice) with a Labsonic M sonicator (Sartorius), and centrifuged at 18,000 rpm for 30 min at 4ºC. Supernatants were mixed with 4 ml of 50% slurry Ni-NTA agarose (Quiagen) equilibrated in binding buffer, and the mixture was incubated at 4ºC for 4 hours on a rotating wheel. Lysate and beads were poured onto Biorad Poly-Prep Chromatography columns for washing and elution steps. Beads were washed once with 5 ml of binding buffer and once with 10 ml of a solution containing 9% of elution buffer (20 mM Tris-HCl pH 7.9, 500 mM imidazole, 500 mM NaCl). Proteins were eluted with a gradient from 100 mM to 400 mM of imidazole (20-80% of elution buffer) in seven fractions of 0.8 ml. Fractions containing recombinant proteins were pooled and dialyzed against 20 mM Tris-HCl pH 7.5, 150 mM NaCl.

For kinase assays, a version of Ppk18 C-terminally tagged with 13 myc epitopes was immunoprecipitated from extracts of $3x10^8$ yeast cells grown in YES treated with rapamycin for 1 hour at 25ºC. Cells were lysed using a Fast-Prep (3 cycles at 5.5 speed, 15 s on, 15 s off) in HB buffer (25 mM MOPS pH 7.2, 60 mM ß-glicerophosphate, 15 mM $MgCl_2$, 1 mM DTT, 1% Triton X-100, 15 mM pNPP and 5 mM EGTA) supplemented with Complete EDTA-free Protease inhibitor cocktail (Roche) and 1 mM PMSF. Extracts were cleared by centrifugation at 13,200 rpm at 4ºC, and the supernatants were incubated with 2.5 µg of anti-c-Myc monoclonal antibody (clone 9E10, Sigma) on ice for one hour, followed by 50 minutes with 60 µl of 50% slurry A/G agarose (Santa Cruz) equilibrated in HB buffer, on a rotating wheel at 4ºC. Beads were washed 5 times with 0.8 ml of HB buffer, and twice with 0.8 ml of kinase buffer (20 mM HEPES pH 7.6, 10 mM $MgCl_2$, 3 mM ß-mercarptoethanol). Kinase assays were performed by incubating 1/3 of the IP with 20 µl of kinase buffer supplemented with 50 µM ATP, 2 µCi of (γ-^{32}P)-ATP and 3 µg of purified 6xHis-Igo1 or 6xHis-Igo1-S64A, at 30ºC for 30 minutes. Reactions were stopped by adding 20 µl of 2X Laemmli protein sample buffer and boiling for 5 minutes. Samples were run on 13% polyacrylamide gels. After running, the gels were dried and exposed to X-ray films at -80ºC.

PP2A·Pab1 phosphatase assays

Recombinant Igo1 and Igo1-S64A mutant proteins for this experiment were purified from 80 ml of *E. coli* BL21(DE3) codon+ PR strain, grown for 16 hours at 18ºC in LB containing 0.1 mM IPTG. The bacteria cells were harvested by centrifugation, resuspended in 4 ml of extraction buffer (20 mM Tris-HCl pH 7.5, 150 mM NaCl, 0.1% Tween 20, 0.1 mM DTT, 0.1 mM EGTA, 2 mM Benzamidine, 20 mM imidazole) containing 2 mM PMSF and a trace of lysozyme, incubated at 37ºC for 5 minutes until the solution become slimy with occasional inverting, cooled down on ice, sonicated (three cycles of 20 seconds, on ice), splitted into 4 x 1.5 ml eppendorf tubes and centrifuged at 14,000 rpm for 10 min at 4ºC. Supernatants (approximately 4 ml) were mixed with 150 µl of 50% slurry Ni beads (HisPur Ni-NTA, Thermo) equilibrated in extraction buffer, and the mixture was incubated for 20 minutes at 4ºC on a rotating wheel. The beads were washed three times in extraction buffer containing 40 mM imidazole and then 400 µl of ATP-Mg^{2+} buffer (20 mM Tris-HCl pH 7.5, 150 mM NaCl, 0.1% Tween 20, 0.1 mM DTT, 0.1 mM EGTA, 40 mM imidazole, 3 mM ATP, 5 mM $MgSO_4$) were added to the beads and incubated on a rotating wheel at 37ºC for 60 minutes. The beads were washed twice in 20 mM Tris-HCl pH 7.5, 150 mM NaCl, 0.1% Tween 20, 0.1 mM DTT, 0.1 mM EGTA, 40 mM imidazole, transfered to open spin columns and the proteins were eluted with 150 µl of buffer containing 50 mM, 75 mM, 100 mM, 125 mM, 150 mM and 200 mM imidazole (three cycles for each imidazole concentration). Fractions containing recombinant proteins were pooled and dialyzed against 25 mM Tris-HCl pH 7.5, 0.1% Triton X-100, 0.2 mM EGTA, 0.1 mM ß-mercaptoethanol and concentrated into 75 µl to a final concentration of 1 mg/ml.

30 µg of recombinant Igo1 or Igo1-S64A proteins were thio-phosphorylated *in vitro* using 0.6 µg of *Xenopus* purified Greatwall, derived from okadaic acid-treated Sf9 insect cells in 20 mM Tris-HCl pH 7.5, 50 mM NaCl, 2 mM ATP-γ-S, 1 mM DTT, 20 mM ascorbic acid sodium salt, 5 mM $MgCl_2$, 7.5 mM KCl, 0.05 mg/ml BSA and 10 µM $MnCl_2$ in 60 µl total volume at 30ºC overnight. 2 µl of each reaction were run on a 15% SDS-PAGE containing 10 µM Phos-Tag. About 80% of wild-type Igo1 was thio-phosphorylated by Greatwall in this reaction, whereas Igo1-S64A mutant protein was not. To remove the free phosphate contaminating the ATP-γ-S, 30 µl of the reaction mix were centrifugated at 735xg for 1 minute through an Illustra MicroSpin G-25 column (GE healthcare). The final protein concentration for each sample was 0.25 mg/ml, which corresponds to 16 µM.

GST-Pab1, expressed under the *nmt1(41)* promoter, was immunoprecipitated from extracts of $4x10^8$ yeast cells grown in EMM. One extract from $4x10^8$ wild-type cells grown in EMM was processed in parallel during the GST purification and used as a negative control. Cleared lysates made in HB buffer (25 mM MOPS pH 7.2, 60 mM ß-glycerophosphate, 15 mM MgCl2, 1 mM DTT, 1% Triton-X100, 15 mM pNPP, 5 mM EGTA, supplemented with complete EDTA free protease inhibitor cocktail-Roche- and 1 mM PMSF) were incubated with Glutathione Sepharose (GE Healthcare) on a rotating wheel at 4ºC for 3 hours. Beads were washed three times with HB and three times in 20 mM Tris-HCl pH 7.5, 5 mM $MgCl_2$, 0.02% ß-mercaptoethanol, 1 mM EGTA. The beads were sedimented at 1200 rpm for 5 seconds and incubated in elution buffer (20 mM Tris-HCl pH 7.5, 150 mM NaCl, 0.01% NP-40, 1mM DTT, 10 mM glutathione) at 4ºC on a rotating wheel. After sedimentation the eluate was retrieved into new tubes. Elution was repeated once. More than 50% of the GST-Pab1 was eluted from the beads.

PP2A-Pab1 phosphatase reactions were performed in a final volume of 10 µl using 1 µl of eluted GST-Pab1 (1:2 dilution), 2 µl of 5x phosphatase buffer (125 mM Tris-HCl pH 7.5, 500 mM NaCl, 1 mM EGTA, 0.25% Triton X-100, 50% glycerol and 0.5 mM ß-mercaptoethanol), 5 µl of Igo1 or Igo1-S64A mock or treated with Greatwall (final concentration 240 nM) and started by adding 2 µl of 1 mM Promega Ser/Thr phosphatase substrate (Promega #V2460, 1mM in water). The reactions were incubated for 1 hour at 37ºC. Free phosphate released by the phosphatase reaction was measured by the addition of 60 µl of BioMol Green (ENZO #BML-AK111) after 20 minutes at room temperature. Absorbance at 620 nm was measured in a 10-mm path cuvette (Violamo, #1-2956-01) using a NanoDrop.

Mathematical model of the fission yeast cell cycle with nutritional mitotic control

Brief description of the core fission yeast model. The core of the fission yeast cell cycle control model is based on our previous work [S3-S5, 41]. The model describes the regulation of the only essential Cdk1:cyclin B complex (Cdk1:Cdc13) that can drive an ordered cell cycle progression in fission yeast (Figure S5). The rate of Cdc13 synthesis, and thereby the production of Cdk1:Cdc13 dimers, is assumed to be proportional to cell mass. The Cdk1:Cdc13 regulatory network is divided into three functional modules responsible for different cell cycle transitions:

- The stoichiometric inhibitor, Rum1, keeps Cdk1 activity low in G1 phase, and it determines the timing of G1/S transition.
- Inhibitory Cdk1 phosphorylation controlled by Wee1 and Cdc25 regulates G2/M transition.
- Cdk1:Cdc13-activated APC/C is responsible for meta/anaphase transition, including Cdc13 degradation.

In G1 phase, Rum1 binds to Cdk1:CycB complexes and inhibits their activities [S6,S7]. Since Rum1 is targeted for rapid ubiquitin-dependent degradation by Cdk1 phosphorylation [S8], Cdk1 and Rum1 mutually inhibit each other (Rum1⊣Cdk1⊣Rum1). By Cdk1 inhibition Rum1 also promotes Cdc13 degradation during G1 phase by keeping APC/C^{Ste9} active [S9]. To keep the model simple, this mechanism is described by rapid Cdc13 degradation from Rum1:Cdk1:Cdc13 trimers (Figure S5) as suggested in the literature [S10]. As a consequence of Rum1-Cdk1 antagonism, Rum1 keeps both the Cdc13 level and Cdk1 activity low in G1 phase (red solid segments on Figures 7B, 7C and 7D). The Rum1 dominance over Cdk1 is terminated at a critical cell mass, since the level of Cdk1:Cdc13 dimers is increasing with cell growth.

Wee1-dependent Cdk1 inhibitory phosphorylation keeps Cdk1:Cdc13 activity at an intermediate level during S and G2 phases (yellow segments on Figures 7B, 7C and 7D). Cdk1-dependent Wee1-inhibition and Cdc25-activation creates a double-negative (Wee1⊣Cdk1⊣Wee1) and a positive feedback (Cdc25 $\rightarrow$ Cdk1 $\rightarrow$ Cdc25) loop. Cdk1 becomes activated at the G2/M transition as a result of turning on these feedback loops at a critical cell mass.

The meta/anaphase module is based on a time-delayed negative feedback loop because Cdk1 promotes its own inactivation through APC/C-dependent Cdc13 degradation. This time-delayed negative feedback destabilises the high Cdk1 activity steady state corresponding to M phase (green segments on Figures 7B, 7C and 7D) by generating a limit cycle oscillation. The limit cycles are born at small cell mass (green dashed lines on Figures 7B, 7C and 7D), but the Cdk1 oscillations are blocked by the low (red segment) and intermediate (yellow segment)

stable steady states created by the G1/S and G2/M modules. Once the cell becomes larger than the critical size dictated by the G2/M size control, Cdk1 activity overshoots the unstable steady state (dashed green segments). APC/C-induced Cdc13 degradation turns on when Cdk1 activity hits the peak value (upper green circles). The drop of Cdk1 activity signals cell division, which resets the cell to half its mass.

A model of the fission yeast Greatwall-Endosulfine-PP2A pathway. PP2A activity is inhibited by its stoichiometric inhibitor, phosphorylated Igo1 (ENSA), but recent experimental evidence suggests that ENSAp is dephosphorylated by PP2A itself [S11]. Therefore ENSAp inhibits the dephosphorylation of other PP2A substrates by "unfair competition" [S11]. ENSAp (Igo1p) is therefore both an inhibitor and a substrate of PP2A, which is implemented in our model by the following reaction:

A steady state assumption for the Igo1:PP2A complex:

$$\text{Igo1p + PP2A} \underset{k_{d55}}{\overset{k_{a55}}{\rightleftharpoons}} \text{Igo1p:PP2A} \xrightarrow{k_{pp2a}} \text{Igo1 + PP2A}$$

$$\frac{k_{d55} + k_{pp2a}}{k_{a55}} = K_M^{pp2a} = \frac{[Igo1p] \cdot [PP2A]}{[Igo1p{:}\,PP2A]} =$$

$$= \frac{([Igo1p]_T - [Igo1p{:}\,PP2A]) \cdot ([PP2A]_T - [Igo1p{:}\,PP2A])}{[Igo1p{:}\,PP2A]}$$

where $[PP2A]_T$ = [PP2A] + [Igo1p:PP2A] and $[Igo1p]_T$ = [Igo1p] + [Igo1p:PP2A] allows us to calculate the level of free PP2A:

$$[PP2A] = [PP2A]_T - [Igo1p{:}\,PP2A] = [PP2A]_T - \frac{\beta - \sqrt{\beta^2 - 4[Igo1]_T[PP2A]_T}}{2}$$

where $\beta = [Igo1p]_T + [PP2A]_T + K_M^{pp2a}$.

The change in the level of $Igo1p_T$ follows the differential-equation (DE):

[[[where Gwp is the Cdk1-phosphorylated, active form of Greatwall-kinase (Ppk18). Experiments with *Xenopus* oocytes suggest that Greatwall is only active if phosphorylated by Cdk1 [S12]. The Cdk1 regulation of Greatwall (Ppk18) is responsible for oscillations of PP2A activity in the model. We further assume that the growth-regulated protein-kinases (Tor and PKA) convert the Cdk1 unphosphorylated Greatwall into a form that cannot be activated by Cdk1 (GW_i), with a rate proportional to the relative growth rate (μ). By assuming a constant level of Greatwall-kinase (GW_{total}) the dynamics of its three forms can be described by two DEs:

$$\frac{d\,[Gw]_i}{dt} = \mathrm{k}_{imu} \cdot \mu \cdot ([\mathrm{GW}]_{\mathrm{total}} - [\mathrm{Gw}]_i - [\mathrm{Gwp}]) - \mathrm{k}_{\mathrm{amu}} \cdot [\mathrm{Gw}]_i$$

$$\frac{d\,[Gwp]}{dt} = \mathrm{k}_{\mathrm{gwa}} \cdot [\mathrm{Cdk1}] \cdot ([\mathrm{GW}]_{\mathrm{total}} - [\mathrm{Gw}]_i - [\mathrm{Gwp}]) - \mathrm{k}_{\mathrm{gwi}} \cdot [\mathrm{Gwp}]$$

where Gw_i and Gwp are the forms of Greatwall inactivated by TOR (PKA) and phosphorylated (activated) by Cdk1, respectively. The unphosphorylated form of Greatwall (GW) is calculated by the conservation equation: $GW = GW_{total} - Gw_i - Gwp$.

Based on the genetic evidence that PP2A promotes Cdk1 inhibitory phosphorylation, we propose that PP2A dephosphorylates both tyrosine-modifying enzymes, Wee1 and Cdc25. This way the Greatwall-Endosulfine-PP2A pathway provides the link between growth and cell cycle controls.

We also assume that the levels of both Igo1 and PP2A are genetically upregulated at slow growth rates. The increased level of PP2A is only required to explain that *igo1Δ* cells are larger in poor medium than wild type cells in rich medium. The simultenous upregulation of Igo1 at slow growth rates in wild type cancels out the mitotic delay effect of PP2A. Since these adaptive changes in the cellular levels of PP2A and Igo1 are supposed to be slow, we are only using the corresponding equations to estimate the cell sizes during balanced growth and division, but not for the nutrional shift experiments.

The cell cycle control network of the fission yeast cell cycle was converted into a set of differential and algebraic equations that were solved numerically by freely available software XPPAUT (http://www.math.pitt.edu/~bard/xpp/xpp.html). Kinetic parameter values and initial conditions are specified in the file below, which can be used by XPPAUT directly to simulate the wild type fission yeast cell cycle progression in rich medium (with a cycle time of 150 min). To simulate the cell cycle progression in poor medium set the relative growth rate (mu) to e.g. 0.325, which gives a 463 min long cell cycle. To simulate *igo1Δ* mutants set the kigo1p parameter to zero.

To calculate the dependence of steady state as a function of cell mass (one-parameter bifurcation diagrams on Figures 7A, 7B and 7C) the following modifications must be implemented in the code: the cell mass (M) DE and the 'global statement' for dividing 'M' by two at cell division need to be removed, and 'M' has to be converted into a parameter.

```
# .ode code of a mathematical model for the fission yeast cell cycle with nutritional control
# initial conditions for dynamic variables
initial CycBT=0.545, Cdk1=0.085, pCdk1=0.447, Complex=0, Wee1=0.99, Cdc25P=0, APC=0, IE=0, CKIT=0.014, GWi=0.943, GWP=0.04, Igo1pT=0.198, M=0.713
# the core fission yeast cell cycle model ----------
# CycBT represents the sum of all Cdk1:Cdc13 forms
CycBT' = kscyc*M - (kdcyc' + kdcyc''*APC)*CycBT - kdcyc"*(Complex + Complex2)
# Cdk1 and pCdk1 represent unphosphorylated and phosphorylated Cdc2:Cdc13 complexes, respectively
Cdk1' = kscyc*M  - kwee*Cdk1 + k25*pCdk1 - (kdcyc' + kdcyc''*APC)*Cdk1 - kass*Cdk1*CKI + (kdiss + Vdcki)*Complex
pCdk1' = kwee*Cdk1 - k25*pCdk1 - (kdcyc' + kdcyc''*APC)*pCdk1 - kass*pCdk1*CKI + (kdiss + Vdcki)*Complex2
# CKIT represents the total level of stoichiometric Cdk inhibitor, Rum1
CKIT'  = kscki - Vdcki*CKIT
# Complex and Complex2 correspond to unphosphorylated and Y-phosphorylated Cdc2:Cdc13:Rum1 trimers, respectively
Complex' = - kwee*Complex + k25*Complex2 - (kdcyc' + kdcyc''*APC + kdcyc")*Complex + kass*Cdk1*CKI - (kdiss + Vdcki)*Complex
Complex2 = CycBT - Cdk1 - pCdk1 - Complex
```

```
CKI = CKIT - Complex - Complex2
# Wee1 and Cdc25P are the active forms of the tyrosine-modifying enzymes (Wee1/Mik1 and Cdc25)
Wee1' = (Vawee' + Vawee"*PP2A)*(1 - Wee1)/(Jwee + 1 - Wee1) - Viwee*Cdk1*Wee1/(Jwee + Wee1)
Cdc25P' = Va25*Cdk1*(1 - Cdc25P)/(J25 + 1 - Cdc25P) - (Vi25' + Vi25"*PP2A)*Cdc25P/(J25 + Cdc25P)
# APC/C is activated by Cdc2:Cdc13 complex indirectly (through IE)
IE'   = kaie*(1-IE)*Cdk1/(Jie + 1 - IE) - kiie*IE/(Jie + IE)
APC'= kaapc*IE*(1-APC)/(Japc + 1 - APC) - kiapc*APC/(Japc + APC)
# exponential growth of cell mass is assumed with minimal cycle time of 150 mins (mumax=0.0046)
# relative growth rate (mu) has values between 0 and 1 (rich medium: mu=1, poor medium: mu=0.325)
M'    = mu*mumax*M
# the cell divides when the active Cdk1:Cdc13 complex drops below a threshold value (thres)
global -1 {Cdk1-thres} {M=0.5*M}
# Rate functions
Vdcki = kdcki' + kdcki"*Cdk1
kwee  = kwee' + (kwee" - kwee')*Wee1
k25   = k25' + (k25" - k25')*Cdc25P
# the model for the growth rate regulated Greatwall/Endosulfine/PP2A pathway----------
# Gwi represents the form of Gw inactivated by PKA and TOR kinases
Gwi' = kimu*mu*(GWtotal - Gwi - Gwp) - kamu*Gwi
# Gwp is the Cdk1:Cdc13 activated form of Greatwall-kinase
Gwp' = kgwa*Cdk1*(GWtotal - Gwi - Gwp) - kgwi*Gwp
# the level of Igo1pPP2A complex (Igo1p:PP2A) is assumed to be in pseudo-steady state
BB  = Igo1pt + PP2At + (kd55 + kpp2a)/ka55
Igo1pPP2A = (BB - sqrt(BB^2 - 4*Igo1pt*PP2At))/2
PP2A = PP2At - Igo1pPP2A
aux PP2A = PP2At - Igo1pPP2A
# the total level of Igo1 (Igo1) is regulated by the growth rate (it is set to 5 at maximal growth rate)
Igo1t = Igo1tot - (Igo1tot - 5)*mu
# Igo1 (Igo1) is phosphorylated by Gwp and dephosphorylated by PP2A
Igo1pt' = kIgo1p*Gwp*(Igo1t - Igo1pt) - kpp2a*Igo1pPP2A
# the total level of PP2A is dependent on relative growth rate (it is set to 1 at maximal growth rate)
PP2At = PP2Atot - (PP2Atot - 1)*mu
# values of kinetic parameter
par kscyc=0.05, kdcyc'=0.05, kdcyc"=0.25, kdcyc'"=0.5, kaie=0.1, kiie=0.025, Jie=0.01, kaapc=0.5, kiapc=0.125, Japc=0.01
par kscki=0.1, kdcki'=0.3, kdcki"=80, kass=100, kdiss=0.1, mu=1, mumax=0.0046, thres=0.06
par kwee'=0.1, kwee"=1, Vawee'=0.1, Vawee"=0.15, Viwee=1, Jwee=0.01,
par k25'=0.1, k25"=4, Va25=1, Vi25'=0.1, Vi25"=0.15, J25=0.01
par kpp2a=1, Igo1tot=9, PP2Atot=1.75, kd55=1, ka55=100, GWtotal=1, kamu=0.06, kimu=1, kgwa=1, kgwi=0.1, kIgo1p=1
@ total=300, dt=0.25, meth=STIFF, xlo=0, xhi=300, ylo=0, yhi=1
@ NPLOT=8,yp=Cdk1,yp2=CycBT,yp3=APC,yp4=CKIT,yp5=GWp,yp6=Igo1pt,yp7=m,yp8=PP2A
@ NTST=15,NMAX=100000,NPR=1000,DS=0.01
@ DSMAX=0.01,DSMIN=0.001,PARMIN=0,PARMAX=2
@ AUTOXMIN=0,AUTOXMAX=1,AUTOYMIN=0,AUTOYMAX=1
done
```

Supplemental references

S1. Harlow, E., and Lane, D. (1988). Antibodies: a laboratory manual. Cold Spring Harbor Laboratory.

S2. Foiani, M., Marini, F., Gamba, D., Lucchini, G., and Plevani, P. (1994). The B subunit of the DNA polymerase alpha-primase complex in *Saccharomyces cerevisiae* executes an essential function at the initial stage of DNA replication. Mol. Cell. Biol. *14,* 923- 933.

S3. Novak, B., Pataki, Z., Ciliberto, A., and Tyson, J.J. (2001). Mathematical model of the cell division cycle of fission yeast. Chaos *11,* 277-286.

S4. Novak, B., and Tyson, J.J. (1997). Modeling the control of DNA replication in fission yeast. Proc. Natl. Acad. Sci. U S A *94*, 9147-9152.

S5. Tyson, J.J., and Novak, B. (2001). Regulation of the eukaryotic cell cycle: molecular antagonism, hysteresis, and irreversible transitions. J. Theor. Biol. *210,* 249-263.

S6. Correa-Bordes, J., and Nurse, P. (1995). $p25^{rum1}$ orders S phase and mitosis by acting as an inhibitor of the p34cdc2 mitotic kinase. Cell *83,* 1001-1009.

S7. Moreno, S., and Nurse, P. (1994). Regulation of progression through the G1 phase of the cell cycle by the rum1+ gene. Nature *367*, 236-242.

S8. Benito, J., Martin-Castellanos, C., and Moreno, S. (1998). Regulation of the G1 phase of the cell cycle by periodic stabilization and degradation of the $p25^{rum1}$ CDK inhibitor. *EMBO J*. **17**, 482-497.

S9. Blanco, M.A., Sanchez-Diaz, A., de Prada, J.M., and Moreno, S. (2000). APC(ste9/srw1) promotes degradation of mitotic cyclins in G(1) and is inhibited by cdc2 phosphorylation. EMBO J. *19,* 3945-3955.

S10. Correa-Bordes, J., Gulli, M.P. and Nurse, P. (1997). $p25^{rum1}$ promotes proteolysis of the mitotic B-cyclin $p56^{cdc13}$ during G1 of the fission yeast cell cycle. EMBO J. *16,* 4657-4664.

S11. Williams, B.C., Filter, J.J., Blake-Hodek, K.A., Wadzinski, B.E., Fuda, N.J., Shalloway, D., and Goldberg, M.L. (2014). Greatwall-phosphorylated Endosulfine is both an inhibitor and a substrate of PP2A-B55 heterotrimers. eLife *3,* e01695.

S12. Blake-Hodek, K.A., Williams, B.C., Zhao, Y., Castilho, P.V., Chen, W., Mao, Y., Yamamoto, T.M., and Goldberg, M.L. (2012). Determinants for activation of the atypical AGC kinase Greatwall during M phase entry. Mol. Cell. Biol. *32,* 1337-1353.